HIV-1 preintegration complex preferentially integrates the viral DNA into nucleosomes containing trimethylated histone 3-lysine 36 modification

Nicklas Sapp[1,2, 3], Nathaniel Burge[5,6], Khan Cox[5,6], Santosh Thapa[1,2], Prem Prakash[1,2], Muthukumar Balasubramaniam[1,2], Devin Christenson[8], Min Li[6], Jared Linderberger[7], Mamuka Kvaratskhelia[7], Wesley Sundquist[8], Jui Pandhare[1,3,4], Robert Craigie[6], Michael G Poirier[4,5], and Chandravanu Dash[1,2*]

From

[1]The Center for AIDS Health Disparities Research
[2]Department of Biochemistry, Cancer Biology, Pharmacology and Neuroscience
[3]School of Graduate Studies and Research
[4]Department of Microbiology, Immunology, and Physiology
Meharry Medical College, Nashville, TN, USA.

[5]Department of Chemistry and Biochemistry, [6]Department of Physics
Ohio State University, Columbus, OH, USA

[6]Laboratory of Molecular Biology,
National Institutes of Diabetes, and Digestive, and Kidney Diseases,
National Institutes of Health, Bethesda, MD, USA

[7]Division of Infectious Diseases
University of Colorado, Aurora, CO, USA.

[8]Department of Biochemistry
University of Utah, Salt Lake City, UT, USA.

[*]Corresponding Author

Chandravanu Dash, PhD
Old Hospital Bldg-CAHDR, Room 5027,
1005 Dr. DB Todd Jr Blvd., Nashville, TN 37208, USA.
E-mail: cdash@mmc.edu
Tel: 615-326-6996

Key Words

Human immunodeficiency virus (HIV), Preintegration complex (PIC),

Nucleosome, Integration, Chromatin, Histone, Post-translational modification (PTM), H3K36me3

Abstract

HIV-1 DNA integration into the host chromosomes is carried out by the preintegration complex (PIC). The PIC contains the viral DNA, virally encoded integrase enzyme and other critical viral/host factors. The PIC-associated viral DNA is preferentially integrated into gene bodies of actively transcribing genes. Here, we identify a biochemical mechanism underlying the preference of PIC-mediated viral DNA integration (PIC-VDI). Specifically, we observed that the PIC-VDI into human chromatin is preferred over the genomic DNA. Surprisingly, nucleosome core particles without any histone modifications were not preferred for PIC-VDI when compared to the analogous naked DNA. However, PIC-VDI was markedly enhanced with nucleosomes containing the trimethylated histone 3 lysine 36 (H3K36me3), an epigenetic mark linked to HIV-1 DNA integration preference. Interestingly, we observed that nucleosomes with flanking linker DNA promoted PIC-VDI in the presence of LEDGF/p75. We also discovered that nucleosomes with linker DNA and H3K36me3 served as the optimal substrate for PIC-VDI. Mapping of the integration sites within these substrates suggest preference of specific regions of the nucleosome core DNA for integration. Finally, we provide biochemical and genetic evidence that histone H1 protein, that condenses the chromatin, negatively regulates HIV-1 DNA integration, consistent with the integration preference for *open chromatin* structure. Collectively, these results identify the role of specific chromatin marks that drive HIV-1 integration preference and define the optimal substrate requirement for efficient DNA integration by the PIC.

Introduction

HIV-1, the causative agent of AIDS, has infected approximately 80 million people worldwide, with ~38 million people living with the virus currently (UNAIDS, 2021). Potent antiretroviral therapy (ART) has rendered HIV-1 infection a chronic disease and have significantly reduced the disease burden to AIDS (UNAIDS, 2021). However, ART is not curative and life-long ART can cause severe toxicity and comorbid conditions [1]. Therefore, a clear understanding of the mechanism of HIV-1 replication is key for developing novel and improved therapeutic strategies. HIV-1 infection is dependent on the integration of the reverse transcribed viral DNA into host chromosomes [2-4]. This critical step is carried out by the virally encoded integrase (IN) enzyme in a multistep process [5]. First, IN carries out the 3'-processing of the viral DNA ends and then via a strand-transfer step, the viral DNA is inserted into host genomic DNA [6-9]. This intricate process of DNA integration is carried out by the viral preintegration complex (PIC) which is composed of IN, the viral DNA, and other viral and host factors [10-15]. Accordingly, establishment of the proviral genome is required for generation of progeny virions and ultimately establishment of viral reservoirs, which remains the principal barrier to HIV-1 cure [16-18].

HIV-1 integration is a non-random event that targets specific genic regions of human chromosomes. There is strong evidence that HIV-1 DNA is integrated into hot spots in the genome. While protein-coding genes account for less than 2% of the genome, they represent over half of the detected HIV-1 integration sites [19-25]. Analysis of HIV-1 integration sites reveals consistent genic integration patterns in *open chromatin* across both cell lines and patient derived samples [23,24,26,27]. These preferred regions for integration are characterized by the active transcription of highly expressed genes, gene density, and epigenetic factors characteristic of *open chromatin* [21,25-31]. The chromosomal context of proviral integration is important, as these genomic characteristics influence proviral transcription [32,33]. To carry out viral DNA integration into the genomic hot spots, the HIV-1 PIC must engage and overcome the structural and functional

45 barriers of chromosomal landscape. A single copy of the human genome can extend over two
46 meters, yet it is packaged into a nucleus with an average diameter of 10 μm [34]. This enormous
47 task of genome compaction is achieved by organizing the DNA into a nucleoprotein polymer
48 called chromatin. The basic repeating unit of chromatin is a nucleosome, each of which contains
49 a nucleosome core composed of an octamer of histone proteins (H2A, H2B, H3 and H4) that
50 wraps 1.6 turns of a 147 bp of DNA [34,35]. The nucleosome core is connected to the adjacent
51 nucleosome core by a segment of linker DNA. The linker DNA is often associated with the histone
52 protein (H1) that further compacts the genome [36-38]. In addition to these genomic organization
53 mechanisms, an array of epigenetic modifications on the histone proteins and DNA, add further
54 complexity to the structural and functional landscape of the chromatin [39-41]. Therefore, specific
55 mechanisms within the nuclear environment are required for the PIC to successfully insert the
56 viral DNA into the hot spots.

57 Despite the targeting of HIV-1 DNA into genic regions for integration, the contribution of
58 chromatin to HIV-1 integration has been elusive. Nevertheless, there is evidence that retroviral
59 INs, including that of HIV-1, specifically target the DNA wrapped within nucleosomes for
60 integration [42-46]. Notably, retroviral INs preferentially target the outward facing major groove of the
61 nucleosomal DNA [44-47]. The distortion of DNA as it bends around the histone octamer is thought
62 to facilitate integration into the nucleosomes. Interestingly, retroviral INs differ in how they
63 integrate viral DNA within chromatinized DNA templates [48-54]. While HIV and MLV target
64 nucleosome cores, some reports show that nucleosome arrays are less preferred for integration
65 when compared to analogous naked DNA[50,53,55]. In contrast, ALV IN activity is specifically
66 enhanced by nucleosome compaction[48]. Evidently, host proteins such as LEDGF/p75, BET, and
67 others also play key roles in viral DNA integration, especially with chromatin substrates [48-50,53,55-
68 58]. Particularly, the interaction between HIV-1 IN and LEDGF/p75 is linked to integration site-
69 selection to genes and can specifically stimulate HIV-1 IN strand-transfer reactions *in vitro* [59-70].

70 Still, the molecular and biochemical details underlying retroviral DNA integration in the context of
71 chromatin are not fully understood.

72 Here we report a biochemical mechanism for the preference of the HIV-1 DNA integration
73 into *open chromatin*. Using HIV-1 PICs extracted from acutely infected T-cell lines, we quantified
74 enhanced viral DNA integration activity with isolated chromatin. However, analysis of PIC-
75 mediated integration with biochemically assembled nucleosomes without histone tail
76 modifications showed reduced integration. Notably, the addition of a tri-methylated histone tail
77 resulted in enhanced PIC-associated viral DNA integration into nucleosomes. Interestingly,
78 addition of linker DNA to nucleosomes regulated the effect of LEDGF/p75 on HIV-1 integration.
79 Furthermore, chromatin compaction by the linker histone $H1^0$ negatively regulated HIV-1
80 integration. Finally, our sequencing analysis suggest integration preference was favored within
81 distinct regions of the H3K36me3 nucleosomal DNA. Overall, our study provides critical
82 biochemical evidence for HIV-1 PIC-mediated integration preference into *open chromatin*.

Results

Chromatin is the preferred substrate for HIV-1 PIC-mediated viral DNA integration. HIV-1 infection is dependent on integration of the viral DNA into host chromosomes by the pre-integration complex (PIC). It is well-established that HIV-1 DNA is preferentially integrated into gene bodies containing actively transcribing genes [19,20,24,30]. However, the biochemical determinants of integration site preference within the chromatin landscape are not fully understood. To better understand the mechanism of HIV-1 integration into chromatin, we adopted a method that measured PIC-associated viral DNA integration (PIC-VDI) using 300 ng of target substrates from isolated chromatin DNA, de-chromatinized genomic DNA, biochemically reconstituted nucleosome core particles (NCP) with or without linker DNA and the analogous DNA sequences. HIV-1 PICs were extracted from acutely infected SupT1 cells [71-74] and are competent for viral DNA integration *in vitro* (SI-Fig. 1A-B). The PIC-VDI assay is specific since the HIV-1 integrase inhibitor raltegravir (RAL) significantly inhibited the DNA integration activity (SI-Fig. 1B). Chromatin, isolated from HEK293T cells, contained the canonical histone proteins, and lacked detectable levels of cytoplasmic protein markers (Fig. 1A-B and SI-Fig. 1C). Importantly, micrococcal nuclease digestion of the isolated chromatin resulted in a “ladder-like” pattern with the smallest DNA band at 150 base pairs (bp) (Fig. 1C and SI-Fig. 13C), equivalent to the length of DNA wrapped around a nucleosome [34,35,75], suggesting optimal protection of the DNA in our chromatin preparation. In parallel, de-chromatinized DNA obtained by deproteination of the chromatin was used as the analogous genomic DNA (gDNA) substrate (Fig. 1C). To probe the preference of PIC-VDI into these substrates, PICs were incubated with either the chromatin or gDNA preparations containing equivalent amount of DNA and PIC-VDI was measured by *alu*-based nested qPCR [72-74]. Results from these measurements revealed that PIC-VDI was significantly higher with the chromatin substrate compared to the gDNA (Fig. 1D-E). Since the chromatin substrate contains the host factors and histone modifications that are positively associated with HIV-1 integration (SI-Fig. 1C), the preference of PIC-VDI into the chromatin is

109 likely driven by the structural elements of nucleosomes such as chemical modifications of histone
110 tails.

111 **Nucleosome core particles (NCP) without histone tail modifications are not**
112 **preferred for PIC-VDI.** There is evidence that nucleosomes- the organizing unit of chromatin, are
113 the preferred substrates of retroviral integration [43-46,49,76]. Therefore, to better understand the
114 enhanced PIC activity with chromatin, we probed PIC-VDI using biochemically assembled NCPs
115 [77]. NCPs were assembled using the Widom 601 nucleosome positioning sequence (NPS) DNA
116 [78] and human histone octamers assembled by a stepwise approach using purified recombinant
117 histone H2A, H2B, H3, and H4 (Fig. 2A). The 147 bp NPS-DNA (Fig. 2B) was added to the
118 assembled histone octamer (Fig. 2C) and formation of the NCP was confirmed by an
119 electromobility shift assay (EMSA) (Fig. 2D). Then, 300 ng of the nucleosome core particle and
120 the nucleosome positioning sequence were used as substrates to measure PIC-VDI by nested
121 qPCR using specific primers that amplify the junctions of integrated viral DNA into the target
122 substrate. Surprisingly, PIC-VDI into the NPS-DNA was significantly higher when compared to
123 the NCP (Fig. 2E). Specificity of these assays were demonstrated by the dramatically reduced
124 PIC-VDI by 1 μM RAL in the presence of both the NCP and NPS (Fig. 2E). There are a number
125 of key differences that could explain why these results deviate from the prior studies showing that
126 nucleosomes are preferred substrates for integration compared to either naked DNA within the
127 same chromatinized plasmid or analogous DNA. One difference is that our study of nucleosome
128 substrates for retroviral DNA integration utilizes HIV-1 PICs compared to the *in vitro* studies of
129 purified HIV-1, MLV, and PFV integrase enzyme [43-46,48-50,55,58]. The PIC associated factors present
130 in our PICs may influence integration preference beyond what might be driven by integrase alone.
131 Further, these studies used nucleosomes, chromatinized substrates and histones derived from
132 cellular sources [34,48-50,53,55,79], whereas our studies use strongly positioned, biochemically
133 assembled recombinant nucleosome. Studies have indicated that the Widom nucleosome

134 position sequence used in our study forms more stable nucleosomes than native DNA
135 sequences[76,78,80].

136 Since we observed reduced PIC-VDI with the NCP substrate, we probed whether this lack
137 of substrate preference is PIC specific. To test this, we used HIV-1 intasomes (INS), which are
138 biochemically assembled complexes of purified integrase with viral DNA sequences from the long
139 terminal repeat (LTR) region [81,82]. We used the purified recombinant IN containing a Ssod7
140 domain for solubility [82] and viral DNA mimics (25 bp and 27 bp) (SI-Fig. 2B). We tested INS-
141 mediated viral DNA integration (INS-VDI) by a qPCR-based assay to amplify the integration
142 junctions into these specific target substrates (SI-Fig. 2B). This qPCR-based approach selectively
143 amplified the viral and target DNA junction only when both the INS and target substrate were
144 added to the reaction mixture (SI-Fig. 2C). Since RAL dramatically reduced the INS-VDI, the
145 assay specifically measures DNA integration (SI-Fig. 2C). Finally, INS-VDI was compared with
146 the NPS and NCP substrates in these assay conditions (Fig. 2F). Surprisingly, VDI was
147 significantly higher with the NPS substrate when compared to the NCP (Fig. 2F), an observation
148 similar to the PIC-VDI (Fig. 2E). Interestingly, the level of reduction in INS-VDI into NCP
149 substrates was ~50% compared to a marked reduction of ~70% in PIC-VDI, suggesting that NPCs
150 confer an additional barrier for PICs to insert the viral DNA. Taken together these observations
151 suggest that NCPs are not preferred for HIV-1 DNA integration by the PIC and the INS.

152 **Trimethylated NCPs at Histone 3 Lysine 36 enhance PIC-VDI.** In the chromatin,
153 nucleosomes are decorated with chemical modifications primarily in the N-terminal tails of the
154 histones [40,83,84]. Given our unexpected results that NCPs without histone modifications are not
155 preferred for PIC-VDI, we assessed whether NCPs containing specific histone tail modifications
156 are required for optimal PIC-VDI. One of the histone modifications commonly associated with
157 HIV-1 integration preference is the trimethylated histone 3 at lysine 36 (H3K36me3) [21,25,26,29-
158 32,51,85]. Therefore, we tested whether the H3K36me3 mark in the nucleosome plays a direct role

159 in HIV-1 integration preference. To test this, we biochemically assembled NCPs with the
160 biochemical mimetic (H3K36$_C$me3) of the H3K36me3 modification generated by an alkylation
161 reaction (Fig. 3A). The H3K36$_C$me3 NCP does not enhance nucleosomal DNA unwrapping [86] and
162 is biochemically indistinguishable from the post-translational modification (PTM) found in cells [87].
163 Our western blot analysis also confirmed the detection of H3K36me3 in isolated chromatin and
164 H3K36$_C$me3 modified NCPs (Fig. 3B). When we tested PIC-VDI using the H3K36$_C$me3-NCP as
165 the substrate, we observed a robust increase in PIC-VDI when compared to the analogous
166 unmodified NCP substrate (Fig. 3C-D). Interestingly, PIC-VDI with the H3K36$_C$me3-NCP
167 substrate was significantly less than the PIC-VDI with the NPS substrate (Fig. 3D). To further
168 probe this paradox, we measured INS-VDI using the NPS, NCP and H3K36$_C$me3-NCP
169 substrates. In stark contrast to the PIC-VDI (Fig. 3C), INS-VDI with the H3K36$_C$me3-NCP
170 substrate showed no measurable difference relative to the unmodified NCP (Fig. 3E). However,
171 the INS-VDI was significantly higher with the NPS substrate when compared to both of the NCP
172 substrates (Fig. 3F). These observations suggest that the biochemical determinants of HIV-1
173 integration in the context of PIC are specific in recognizing the histone H3K36me3 modification in
174 the nucleosome compared to the INS.

175 **LEDGF/p75 addition stimulates INS-VDI but reduces PIC-VDI.** In addition to specific
176 histone modifications, the PIC utilizes several host proteins to efficiently integrate the viral DNA
177 into the host chromosomes [57,88-91]. Early studies identified LEDGF/p75 as the key host protein to
178 support HIV-1 integration [59-62,67-69,79]. LEDGF/p75 binds to the integrase catalytic core domain
179 (CCD) and stimulates the strand-transfer activity of lentiviral integrases, including HIV, with naked
180 and chromatinized substrates [92-94]. Therefore, we tested the effects of LEDGF/p75 on INS-VDI
181 and PIC-VDI using nucleosome and naked DNA substrates. First, increasing amounts of purified
182 LEDGF/p75 was supplemented to the INS-VDI reaction mixture containing the NPS and NCP
183 substrates. We observed a dose dependent enhancement of INS-VDI with the NPS-DNA with

184 increasing concentrations of LEDGF/p75 (Fig. 4A). Similarly, LEDGF/p75 addition also stimulated
185 INS-VDI with the NCP (Fig. 4B). Surprisingly, increasing amounts of LEDGF/p75 did not enhance
186 PIC-VDI with the NPS substrate albeit a slight but non-significant decrease at the highest
187 concentrations (Fig. 4C). However, LEDGF/p75 addition significantly reduced PIC-VDI with the
188 NCP (Figure 4D) in contrast to the enhanced effect of the protein in INS-VDI assays (Fig. 4A-B).
189 Notably, our western blot analysis showed that endogenous LEDGF/p75 is present in our PIC
190 preparation (Fig. 4E). Therefore, it is plausible that the PIC-associated endogenous LEDGF/p75
191 levels is sufficient for VDI and additional amounts of the protein has an inhibitory effect. To test
192 this, we used a fluorescence resonance energy transfer (FRET) based binding assay that utilizes
193 a 5'-Cy3 labeled NPS reconstituted into an NCP containing a Cy5 label on the octamer [95,96]. The
194 creative positioning of these two fluorophores allowed for the measurement of NCP accessibility
195 of a test protein near the DNA entry/exit location. Particularly, since LEDGF/p75 is known to bind
196 the NCP at the entry/exit site [86,97,98], this assay is uniquely suited for our experiment. In this assay,
197 a *GAL4* binding sequence was cloned into the NPS (at the nucleotide positions of 6 to 25) to
198 determine GAL4 accessibility to the NCP in direct competition with LEDGF/p75 (SI-Fig. 4A).
199 Initially, we demonstrated that LEDGF/p75 binds to the NCP by EMSA (SI-Fig. 4B) consistent
200 with the published studies [97,98]. Moreover, in the absence of GAL4, addition of increasing amounts
201 of LEDGF/p75 did not alter the FRET efficiency (SI-Fig. 4C). These results established that
202 LEDGF/p75 addition minimally disrupts the interactions between the DNA and histones within the
203 NCP. From our fluorescence polarization analysis, we observed that LEDGF/p75 binds to both
204 the NCP and H3K36$_C$me3 NCP substrates with a comparable affinity of 30 and 28 nM,
205 respectively (Figure 4F). Then we tested the NCP accessibility to GAL4 in the presence of
206 LEDGF/p75 (Fig. 4G-H). Interestingly, LEDGF/p75 addition reduced the accessibility of GAL4 to
207 the NCP by ~2-fold. Similarly, GAL4 accessibility to the DNA in the NCP containing H3K36me3
208 was also reduced by LEDGF/p75. Collectively, these results suggest that LEDGF/p75 can
209 physically or sterically block trans-factors from gaining access to the DNA within the NCP. These

210 data would suggest that LEDGF/p75 reduces PIC-VDI by blocking access of PIC-associated viral
211 DNA to the NCP-bound target DNA.

212 **NCPs containing H3K36me3 and linker DNA promote PIC-VDI.** Our results show that
213 the NCP is less preferred for both PIC-VDI and INS-VDI compared to the analogous NPS-DNA
214 (Fig. 2E-F). To better understand this surprising result, we tested the effect of the NCP on viral
215 DNA integration by adding a 50 bp linker DNA flanking both ends of the NCP-bound DNA (Fig.
216 5A-B, SI-Fig 5A), which is more representative of nucleosomes in chromatin [75,99]. First, we
217 measured INS-VDI with the 247 bp linker NPS-DNA and compared it with the linker NCP (Fig.
218 5C). We observed a reduction in the integration with the linker NCP compared to the linker NPS,
219 similar to our results with NPS and NCP substrates (Fig. 2). Furthermore, INS-VDI with the linker-
220 NCP and the linker H3K36$_C$me3-NCP substrates showed that the histone trimethylation has a
221 negligible effect on viral DNA integration (Fig. 5D). Results from INS-VDI with all of three linker
222 substrates again showed the preference of INS-VDI for the NPS substrate (Fig. 5E),
223 demonstrating that naked DNA is a highly preferred substrate for the HIV-1 INS. Finally, we tested
224 PIC-VDI with the linker NPS-DNA and NCP. The linker NPS was preferred for PIC-VDI over the
225 linker NCP (Fig. 5F), similar to the data of INS-VDI (Fig. 5C-E) and PIC-VDI with non-linker DNA
226 containing substrates (Fig. 3C-D). However, the results of PIC-VDI with the linker NCP and linker
227 H3K36$_C$me3-NCP revealed a significant enhancement in PIC-VDI with the H3K36$_C$me3-NCP
228 substrate (Fig. 5G). Most importantly, comparative analysis of PIC-VDI with all of the linker
229 substrates showed that the linker H3K36$_C$me3-NCP supported significantly higher VDI than the
230 linker NCP and linker NPS-DNA (Fig. 5H). This is in contrast to the results with INS-VDI (Fig. 5E),
231 suggesting that the combination of the H3K36me3 and the presence of linker DNA provide a
232 biochemically favored environment specifically for HIV-1 PIC-VDI. These results provide the first
233 biochemical evidence for the H3K36me3-mediated stimulation of HIV-1 integration by the PIC.

234 Furthermore, these data also indicate the PIC contains the necessary host factors to support such
235 stimulation compared to the INS.

236 **LEDGF/p75 selectively stimulates PIC-VDI into specific substrates.** Our results
237 indicated that the nucleosome features (histone tail modification and DNA length) and the
238 chromatin binding proteins (LEDGF/p75) directly regulate viral DNA integration. Particularly, the
239 combination of the H3K36me3 and linker DNA within the NCP have an additive effect on PIC-VDI
240 (Fig. 5H). This is in contrast to the PIC-VDI into non-linker NCP that showed a dramatic reduction
241 in the presence of LEDGF/p75 (Fig. 3F). To better understand these paradoxical effects of
242 LEDGF/p75, we measured PIC-VDI using the linker substrates in the presence of LEDGF/p75.
243 We observed that with the H3K36me3-NCP (lacking linker DNA), LEDGF/p75 addition did not
244 inhibit VDI, rather it resulted in a slight increase in PIC-VDI (Fig. 6A). Comparison of this data with
245 the unmodified-NCP indicate that PIC-VDI is supported in the presence of H3K36me3. Moreover,
246 the addition of LEDGF/p75 to the H3K36me3-nucleosome opposed the dramatic reduction in VDI
247 observed with the unmodified-nucleosome (Fig. 6B). Further analysis revealed a 3-fold recovery
248 of PIC-VDI with substrates containing the H3K36me3-NCP over the unmodified-NCP (Fig. 6C).
249 Intriguingly, LEDGF/p75 addition to the unmodified linker NCP resulted in an enhanced PIC-VDI
250 (Fig. 6D), an observation in clear contrast to the dose dependent reduction of PIC-VDI with the
251 unmodified-NCP (Fig. 4D). Finally, we assessed PIC-VDI into the linker H3K36me3-NCP with
252 LEDGF/p75 addition. To our surprise, these results showed no significant effect of LEDGF/p75
253 addition on PIC-VDI (Fig. 6E). Importantly, the raw integration values indicate that the integration
254 quantity is relatively high (SI-Fig. 6C) suggesting that *in vitro* integration maybe occurring at an
255 optimal level with the linker H3K36me3-NCP and exogenous LEDGF/p75. These observations
256 provide further support that the presence of linker DNA and H3K36me3 in an NCP substrate is
257 optimal for HIV-1 integration.

258 **The nucleosome core is preferentially targeted for integration when modified with**
259 **H3K36me3.** Our results identified that nucleosomes with a linker DNA and histone tail
260 modification akin to *open chromatin* optimally enhanced PIC-VDI (Fig. 5H and SI-Fig. 6C). To
261 further study the details of viral DNA insertion into these preferred substrates, we deep sequenced
262 integration reactions with the linker substrates [79]. Duplicate integration reactions of the linker NPS,
263 linker NCP and linker H3K36me3-NCP substrates were PCR amplified, concentrated, and
264 spectrophotometrically analyzed. Amplicons were deep sequenced and we quantified reads that
265 contained sequences of the HIV-1 5' LTR adjoined to the linker sequence for the NPS-DNA, NCP,
266 and H3K36me3-NCP targets. Although the short substrate length caused technical challenges
267 and only allowed us to generate low reads, nevertheless the sequencing data identified integration
268 junctions and suggest distinct integration patterns in each of the linker NPS, linker NCP, and linker
269 H3K36me3-NCP substrates (SI-Fig. 8-10). With the linker NPS, integration junctions were
270 identified throughout the length of the sequence with overrepresentation of viral DNA integration
271 near the target DNA ends (Fig. 7A and SI-Fig. 8). Similarly, the integration junctions were also
272 found in the unbound linker DNA regions of the linker NPC (Fig. 7B and SI-Fig. 9). Notably, the
273 integration junctions within the linker H3K36me3-NCP were identified predominantly in the
274 nucleosome core sequence, in striking contrast to the linker NPS and NCP (Fig. 7C, SI-Fig. 7 and
275 SI-Fig. 10). The location of the integration sites within the linker H3K36me3-NCP are mapped
276 near the entry/exit sites of the NCP (data not shown). Importantly, this is the location of the H3-
277 tail protrusion between the nucleosomal DNA[39,95,98], indicating that the HIV-1 PIC is drawn toward
278 the H3K36me3 mark when engaged with a nucleosome during an integration event. To further
279 understand these sequencing data, we quantified the integration site counts as a percentage of
280 the total integration events. These analyses revealed that the linker NPS and linker NCP
281 comprised ~87 and ~67 % of the junctions within the linker DNA, respectively (Fig. 7D). Distinctly,
282 the linker H3K36me3-NCP contained over ~90 % of the integration junctions adjoined in the
283 nucleosome core sequence. Integration frequencies varied dramatically between the unmodified

284 and H3K36me3-NCP, wherein the nucleosome core of the linker H3K36me3-NCP contained ~95
285 % of the integration junctions (Fig. 7E, SI-Fig. 7B). However, the frequency of integration within
286 the nucleosome core was only ~15 % with the linker NPS-DNA and linker NCP lacking any histone
287 modifications (Fig. 7E, SI-Fig. 7B). Collectively, these results suggest that H3K36me3
288 modification may regulate HIV-1 integration preference within a nucleosome.

289 **Chromatin compacting Histone H1 inhibits HIV-1 DNA integration.** To further study
290 the role of chromatin structure on HIV-1 integration, we next tested effects of H1 protein on HIV-
291 1 DNA integration. It is well-established that H1 reduces chromatin accessibility by facilitating
292 chromatin compaction [37,100] through the direct interaction with the linker DNA near the entry/exit
293 location of the NCP and at the NCP dyad [36,101]. Therefore, we measured HIV-1 DNA integration
294 by both PIC and INS in the presence of increasing concentrations of purified recombinant histone
295 $H1^0$ protein (0-100 nM). Our results revealed that INS-VDI was dramatically reduced in a dose-
296 dependent manner with increasing concentration of $H1^0$ protein (Fig. 8A-C). The inhibitory effect
297 of H1 was universally observed with the linker NPS-DNA, linker NCP and the non-linker NCP.
298 Surprisingly, addition of $H1^0$ protein did not inhibit PIC-VDI at the concentrations of 0-100 nM (Fig.
299 8D-F). Rather with the linker substrates, nM concentrations of $H1^0$ either slightly enhanced PIC-
300 VDI with the linker NPS-DNA or had a minimal effect on PIC-VDI with both the unmodified and
301 H3K36me3 linker NCP substrates (Fig. 8D-F). Then, we tested $H1^0$ addition at saturating
302 concentrations, 287 and 1474 μM, which correspond to a 1:1 or 1:5 molar ratio to the substrate
303 concentrations, respectively. Interestingly, at these saturating concentrations, PIC-VDI was
304 dramatically reduced into the NPS-DNA, NCP and H3K36cme3 NCP substrates containing the
305 linker DNA (Fig. 8G-I). Finally, we tested the effects of H1 on PIC-VDI using chromatin and de-
306 chromatinized gDNA substrates. After preincubating the substrates with saturating concentrations
307 of $H1^0$, we observed significantly reduced PIC-VDI with the genomic DNA and chromatin
308 substrates (Fig. 8J-K, SI-Fig. 13E-F). Notably, nM amounts of $H1^0$ addition did not reduce PIC-

309 VDI with the genomic DNA and chromatin substrates (SI-Fig. 12A-D), highlighting that specific
310 stoichiometry between H1 and the chromatin is required for blocking accessibility of the PIC-
311 associated viral DNA into chromosomal DNA. Collectively, these biochemical results provide
312 further evidence of chromatin structure requirements for efficient HIV-1 DNA integration.

313 **Histone H1 regulates HIV-1 proviral integration.** Our H1 protein addition results shows
314 that $H1^0$ can directly inhibit HIV-1 DNA integration. To test the physiological relevance of this
315 biochemical observation, we probed whether H1 expression regulates HIV-1 DNA integration into
316 human chromosomes in infected cells. To assess the effect of H1 on HIV-1 integration, we
317 overexpressed $H1^0$ in HEK293T cells prior to inoculation with psuedotyped HIV-1 virions. $H1^0$
318 overexpression in these cells were confirmed by western blot analysis (Fig. 9A). The genomic
319 DNA was extracted from the WT and $H1^0$ overexpressing cells and the proviral integration (PVI)
320 was measured by nested Alu-gag PCR method [73,74,102]. Our results revealed that viral DNA
321 integration was significantly reduced in the $H1^0$ overexpressing cells relative to the control cells
322 (Fig. 9B), suggesting a negative correlation between H1 expression and HIV-1 integration. We
323 next carried out knocked-down studies using siRNA-based approach. TZM-bl cells transfected
324 with H1-targeting siRNA showed dramatic reduction in H1 protein expression relative to the non-
325 targeting control cells (Fig. 9C). Measurement of PVI in these cells showed that H1-depletion
326 resulted in a slight increase in HIV-1 DNA integration levels (Fig. 9D), providing further evidence
327 of a negative correlation between H1 protein levels and proviral DNA integration. Collectively,
328 these results illustrate that H1 could play a direct role in blocking HIV-1 integration.

329 **Discussion**

330 HIV-1 infection is dependent on the integration of the viral DNA into genic hotspots of host
331 chromosomes [2]. These hotspots contain actively transcribing genes that are epigenetically
332 marked with histone modifications of *open chromatin* [21,25,26,29-31]. However, the exact role of viral
333 and host factors that program the PIC to integrate the viral DNA into these hotspots remains
334 largely unclear. Furthermore, establishing a direct and functional link between the markers of
335 *open chromatin* and HIV-1 integration preference in cell-based and *in vitro* systems has been
336 challenging [51,53,54,58,103]. Therefore, we employed a biochemical approach involving the extraction
337 of PICs from acutely infected cells and quantified viral DNA integration activity *in vitro* (SI-Fig. 1A-
338 B) [72-74]. We coupled PIC-VDI with biochemical assembled nucleosomes to define target substrate
339 preference for HIV-1 DNA integration. Using this novel approach, we identified that the
340 H3K36me3 histone modification-an epigenetic histone mark of active transcription, plays a direct
341 role in HIV-1 DNA integration preference. Particularly, our results show that nucleosomes
342 assembled with the H3K36me3 histone is a preferred target and HIV-1 DNA integration
343 predominantly occurred within the DNA wrapped around the nucleosome core. The host-factor
344 LEDGF/p75 stimulated HIV-1 DNA integration into the nucleosomes preferentially in the presence
345 of a linker DNA. Finally, the histone H1 protein that induces compaction of chromatin, dramatically
346 reduced HIV-1 DNA integration into nucleosomes, naked DNA and chromatin substrates.
347 Collectively, these studies establish a biochemical link between *open chromatin* structure and
348 HIV-1 integration preference.

349 The molecular and biochemical mechanisms that drive HIV-1 DNA into specific regions of
350 *open chromatin* are not clearly understood. This is in part due to the complexity of the structural
351 landscape of the human chromatin coupled with an unclear understanding of the PIC function and
352 composition. Chromosomes are oligomers of nucleosomes, which regulate access to the genomic
353 DNA, through a number of intrinsic biochemical and structural mechanisms [39-41]. Each

354 nucleosome constitutes the NCP, linker DNA, and a linker histone [34]. The NCP consists of
355 ~147 bps of DNA wrapped in left-handed super helical turns around a histone octamer [35]. The
356 histone octamer contains two copies each of the core histones H2A, H2B, H3, and H4 and the
357 NCPs are connected by stretches of linker DNA [75,99]. Together, the NCP forms a disc-like structure
358 that protects the DNA within the NCP from nucleases [104] and restricts the binding of transcription
359 factors [105,106]. However, these stable nucleosomes must also allow access to the nucleosomal
360 DNA for genomic functions such as DNA replication, RNA transcription and DNA damage repair
361 [107-109]. Evidently, this is achieved through the near meta-stable nature of the NCPs, driven by
362 structural and conformation mechanisms involving: a) the intrinsic binding affinity of the histone
363 octamers, b) post-translational modifications of the histone proteins and the DNA, c) the
364 competitive or cooperative binding of other chromatin binding factors, and d) active translocation
365 by ATP-dependent remodeling complexes. However, the mechanisms by which retroviruses
366 counter the intrinsic structural and conformational barriers to access the nucleosomal DNA to
367 insert the viral DNA is not fully understood. Nonetheless, *in vitro* studies of MLV PICs, together
368 with purified MLV and HIV integrases (IN) show preference of the nucleosomal DNA relative to
369 naked DNA as targets of integration [43-46]. Furthermore, the curvature of nucleosomal DNA bending
370 around the histone octamers or even the histone proteins themselves seem to impact viral DNA
371 integration preference [46,47,54,103,110]. Conversely, integration activity of recombinant HIV-1 IN
372 enzyme can also be reduced with biochemically assembled nucleosomes and chromatin arrays
373 are used as target substrates [50,53,55]. Our results showing enhanced viral DNA integration into
374 extracted chromatin-bound DNA relative to the de-chromatinized genomic DNA (Fig. 1D-E),
375 provides the first biochemical evidence for the substrate preference of the HIV-1 PIC. These
376 results are highly significant given that the PIC is solely responsible for carrying out HIV-1 DNA
377 integration into the host chromosomes to establish life-long infection.

378 To understand the mechanism of chromatin preference for HIV-1 DNA integration, we
379 adapted an *in vitro* reconstitution system to assemble nucleosomes with the Widom 601
380 nucleosome positioning sequence (Fig. 2A-D) [77,78]. This method generates compositionally
381 uniform and precisely positioned nucleosomes compared to the cellular sources that contain
382 highly diverse nucleosomes marked with an array of histone and DNA modifications [40,104,111]. Most
383 importantly, the biochemically assembled nucleosome is uniquely suited to test whether the NCP
384 without any histone tail modification and the analogous NPS-DNA can serve as substrates for
385 HIV-1 DNA integration. To our surprise, we observed higher viral DNA integration with the NPS-
386 DNA rather than the NCP-bound DNA by both HIV-1 PICs and recombinant intasomes (INS) (Fig.
387 2E-F). Since, these NCPs are devoid of any histone tail modifications, our results suggest that
388 the DNA-wrapped around naked nucleosomes lack the biochemical and/or structural
389 determinants to support efficient HIV-1 DNA integration. Furthermore, the NPS-DNA (Widom 601)
390 used in these experiments is optimized for binding to the NCP with high affinity [76,78,80]. This could
391 impose strong steric hindrance for the access and insertion of the viral DNA into NCP-bound DNA,
392 whereas the naked NPS-DNA substrate possess no such biochemical or structural limitation.
393 Notably, the previous studies showing enhanced integration into nucleosome-bound DNA were
394 derived from disparate chromatinized substrates, such as chicken erythrocytes, yeast and SV40
395 mini-chromosomes, a mouse mammary tumor virus sequence mono-nucleosome, and a
396 heterogeneously positioned chimeric di-nucleosome [43-46]. Moreover, the histones used in
397 subsequent nucleosome reconstitution studies were from a cellular source (HeLa cells or chicken
398 erythrocytes) that most likely retained the native post-translational modifications that could
399 influence viral DNA integration [48-50,55,58,79]. Therefore, our results suggest that the DNA wrapped
400 within the NCPs lacking any histone tail modifications or linker DNA sequences is not a preferred
401 substrate for HIV-1 DNA integration.

402 Chromatin structure is broadly categorized into *open* or euchromatin and *closed* or
403 heterochromatin state [75,112]. Heterochromatin represents a highly condensed, gene-poor, and
404 transcriptionally silent state, whereas euchromatin is less condensed, gene-rich, and more easily
405 transcribed [113]. Multiple features of chromatin, including histone modifications, DNA methylation,
406 and small RNAs, are involved in higher order chromatin structure and thus, facilitate or prevent
407 access to the nucleosomal DNA [114,115]. Notably, histone tail modifications characteristic of *open*
408 *chromatin* are positively correlated with HIV-1 DNA integration preference [21,24-26,28-30,85,89].
409 Conversely, histone modifications that define DNA compaction into a heterochromatin state are
410 negatively associated with HIV-1 integration. Particularly, the H3K36me3 modification is positively
411 correlated with HIV-1 DNA integration across a number of published data sets [21,22,25,26,29-32,85,116].
412 Although the underlying mechanism by which H3K36me3 enhances HIV-1 integration targeting
413 is unclear, H3K36me3 is an abundant and highly conserved chromatin modification within the
414 body of transcriptionally active genes [117-119]. H3K36me3 also plays critical roles the regulation of
415 transcription elongation, DNA repair, prevention of cryptic start sites, pre-mRNA splicing and
416 processing [120-123]. Seemingly, H3K36me3 may play a role in tethering the PIC to the actively
417 transcribing genes to facilitate HIV-1 DNA integration through the host factor LEDGF/p75
418 [29,30,51,98,123,124]. Accordingly, we observed higher PIC-mediated DNA integration into the
419 nucleosomes containing H3K36me3 compared to the unmodified NCP (Fig. 3C and Fig. 5G).
420 Quite surprisingly, the level of viral DNA integration into the H3K36me3-NCP was lower compared
421 to the NPS-DNA (Fig. 3D and SI-Fig. 3B). Even though our results cannot fully explain the exact
422 mechanism, the nucleosomes used in our study contain a single histone modification in contrast
423 to the nucleosomes within native chromosomes (or natively sourced histones) that are decorated
424 with a vast array of epigenetic histone and DNA modifications [43-46,48-50,53,55,58,79]. Interestingly, the
425 presence of a linker DNA optimally stimulated PIC-mediated DNA integration into the linker
426 H3K36me3-NCP (Fig. 5H and SI-Fig. 5F). The preference for the linker H3K36me3-NCP by the
427 PICs was not observed with the HIV-1 intasome-mediated viral DNA integration (Fig. 3E-F and

428 Fig. 5D-E), consistent with other studies that reported negligible effects by histone PTMs within
429 chromatinized substrates on HIV-1 intasome activity [51,54,58]. These results revealed that the
430 recognition of H3K36me3 mark is PIC specific and is probably mediated by a viral and/host
431 factor(s) other than the HIV-1 integrase enzyme. Interestingly, the HIV-1 PIC preference for
432 integration with the linker H3K36me3-NCP aligns with studies suggesting HIV-1 IN targeted
433 regions of chromatin arrays (assembled with native histones) with less nucleosome density as
434 such will contain linker DNA [34,50,55]. Taken together, these results suggest that H3K36me3
435 modification in the NCP and flanking linker DNA serve as biochemical determinants for efficient
436 HIV-1 DNA integration.

437 During HIV-1 infection, a number of host factors are utilized to complete the early and late
438 stages of the viral replication cycle [125]. HIV-1 DNA integration into the host chromosomes by the
439 PIC is dependent on host factors such as LEDGF/p75, INI1, CPSF6, and others [89-91,126]. The PIC-
440 associated integrase procures LEDGF/p75 by interacting with the integrase binding domain (IBD)
441 [63,92,94]. Concomitantly, LEDGF/p75 specifically interacts with the H3K36me3-marked chromatin,
442 and other methylated histones, through the PWWP domain and AT-hook motifs [97,98,127]. It has
443 been reported that LEDGF/p75 facilitates HIV-1 DNA integration through these binding
444 interactions by tethering the PIC to actively transcribing genes [49,61,63,67,94,128]. Therefore, we
445 hypothesized that the combination of LEDGF/p75 and the H3K36me3 would yield an additive
446 effect on HIV-1 DNA integration in our *in vitro* assay. Accordingly, significant increase in HIV-1
447 DNA integration into both the NPC and NPS-DNA was observed by the intasomes in the presence
448 of LEDGF/p75 (Fig. 4A-B). Surprisingly, LEDGF/p75 significantly reduced PIC-VDI with the NCP
449 substrate and had minimal effect with the NPS-DNA (Fig. 4C-D). Notably, endogenous
450 LEDGF/p75 is present in the extracted PICs (Fig. 4E), and addition of exogenous LEDGF/p75
451 blocked access to the NCP bound DNA (Fig. 4F-H). Thus, we predict that excessive LEDGF/p75
452 can sterically hinder access of the PIC-associated viral DNA to the NCP-bound target DNA. A

453 lack of such block to the intasome-associated viral DNA, points to the involvement of additional
454 factors and/or mechanisms specific to the PIC. Interestingly, LEDGF/p75 addition to PIC-
455 mediated integration assays with the H3K36me3-NCP substrate relieved the steric block and
456 allowed recovery of the PIC-mediated integration by three-fold (Fig. 6A-C). Furthermore, the
457 presence of the flanking linker DNA that are exposed in *open chromatin*, resulted in the stimulation
458 of PIC-mediated integration by LEDGF/p75 even with the unmodified NCP substrate (Fig. 6D).
459 Collectively, these data implicate that structural and or conformational features of nucleosomes
460 rendered by linker DNA and the H3K36me3 modification are essential for the host factor
461 LEDGF/p75 to promote PIC-mediated viral DNA integration.

462 Our biochemical data shows that the H3K36me3-NCP containing linker DNA is the optimal
463 substrate for PIC-mediated integration. However, our *in vitro* integration assay is not designed to
464 identify the targets of integration into specific regions of the NCP. The NCP-bound DNA is highly
465 contorted and bent into ~1¾ left-handed super helical turns of about 80 bp/turn [34,35]. This bending
466 is a consequence of the minor and major groove structures of the DNA where the minor grooves
467 are preferentially oriented toward the histone octamer surface [34,78,129,130]. Notably, there is
468 evidence that outward-facing DNA major grooves are favored target sites of retroviral integration
469 [45,46] and periodicity for integration occurs at the sites of the major grooves of the target DNA within
470 the nucleosome. Even though, integrases lack DNA sequence specificity for integration targeting
471 [131,132], studies of mono-nucleosome particles [45] or mini-chromosomes [43,44] have shown that the
472 DNA wrapped around the nucleosome are preferentially targeted compared to nucleosome-free
473 DNA. Therefore, to better understand the structural consequence of the H3K36me3-NCP on viral
474 DNA targeting, we carried out deep sequencing of the viral DNA integrants from PIC-VDI assays
475 with the linker NPS-DNA, linker NCP, and the linker H3K36me3-NCP. PIC-mediated viral DNA
476 integration within the linker NPS preferably occurred throughout the DNA sequence and primarily
477 in the linker sequence positions 1–50 bp and 197 – 247 bp (Fig. 7A, SI-Fig. 7 and SI-Fig. 8).

478 Similarly, integration within the linker NCP occurred most frequently in the linker DNA and a slight
479 uptick in the integration sites throughout the nucleosome core positioning sequence, base pairs
480 50 – 197 (Fig. 7B, SI-Fig. 7 and SI-Fig.9). Remarkably, the integration into the nucleosome core
481 DNA increased within the linker H3K36me3-NCP. Both the integration count and frequency
482 occurred overwhelmingly in the nucleosome core sequence of the H3K36me3-NCP with linker
483 DNA (Fig. 7C, SI-Fig. 7 and SI-Fig. 10). It should be noted that these integration site analyses
484 were from sequencing reads of <500, due to the technical challenges of shorter DNA substrates.
485 Therefore, we are cautious about the statistical and physiological significance of these
486 observations. Nevertheless, qualitative analysis of the integration sites within the linker
487 H3K36me3-NCP indicate that the integrants abutted within the super helical location (SHL) -1, -
488 7, +7 and +1, which corresponds to the location where the H3-tail protrudes through the
489 nucleosomal DNA [39,86,98]. This observation suggests a functional role of H3K36me3 mark in
490 directing the HIV-1 PIC-associated DNA into specific regions of the nucleosomal-DNA.

491 We provided biochemical evidence that nucleosome structure characteristic of *open*
492 *chromatin* enhances HIV-1 integration. Interestingly, *open chromatin* represents a minority of the
493 human genomic DNA, whereas the *closed chromatin* or heterochromatin represents up to 80
494 percent of the genomic DNA [112,133]. However, it is unclear why HIV-1 integration is disfavored in
495 these vast DNA regions of the human chromosomes [21,26,28,29,32]. To interrogate the role of closed
496 chromatin on HIV-1 integration, we probed the effects of the linker histone $H1^0$ due to its relatively
497 high abundance among H1 variants [134] and well-characterized ability to condense chromatin fibers
498 and form rigid, stable *chromatosome* structures [36,101]. As expected $H1^0$ addition protected isolated
499 chromatin from micrococcal nuclease digestion (SI-Fig. 13A-D) and at non-saturating amounts,
500 inhibited HIV-1 intasome-mediated viral DNA integration (Fig. 8A-C). This is consistent with the
501 published studies with HIV-1 integrase and H1-mediated condensation of recombinant
502 nucleosome arrays [48,100,135]. Surprisingly, non-saturating amounts of $H1^0$ failed to inhibit PIC-

503 mediated viral DNA integration into the linker substrates (Fig. 8D-F and SI-Fig. 11A-C). However,
504 at stoichiometric saturating levels relative to the DNA substrate, PIC-mediated viral DNA
505 integration was significantly reduced with all the linker substrates (Fig. 8 G-I and SI-Fig. 11D-F),
506 the genomic DNA and the chromatin (Fig. 8 J-K and SI-Fig. 13E-F). Our data indicates that
507 chromatosome formation is essential for the H1-mediated inhibition of PIC-VDI (SI-Fig. G-H).
508 Finally, proviral DNA integration was also reduced in $H1^0$ O/E cells and conversely was enhanced
509 in $H1^0$ depleted cells albeit to a smaller degree (Fig. 9B and 9D). The moderate effect by the
510 reduction the $H1^0$ on HIV-1 integration in the cell-based assays most likely represents the
511 functional redundancy of the H1 variants, some of which could compensate the inhibitory effect
512 of the single variant depletion [136-138]. Notwithstanding, our data suggests that the linker histone
513 H1 can negatively regulate HIV-1 DNA integration most likely through chromatin compaction.

514 In conclusion, our study provides biochemical evidence and mechanistic insights into HIV-
515 1 integration preference into *open chromatin*. For the first time we defined a direct role of the
516 H3K36me3 epigenetic mark in HIV-1 integration preference and identified the optimal substrate
517 for HIV-1 PIC-mediated integration. Finally, our study demonstrates the importance of
518 biochemical studies of the PIC to achieve a clear understanding of the mechanism of retroviral
519 DNA integration.

520

Acknowledgements

This work was supported by the National Institutes of Health grants R01 AI136740, R01 DA 042348, R56 AI122960, R24 DA036420, R25AI1647610, R01AI162694, and U54 MD007586 to C.D., and the support from the Research Centers in Minority Institutions (RCMI) grant U54MD007586 to J.P, as well as the training grants R25 GM059994 and F31 AI150488 support for N.S. This work is also supported in part by the Meharry Translational Research Center (MeTRC) grant U54MD007593 and Tennessee CFAR grant P30 AI110527 from the National Institutes of Health to C.D. M.L. and R.C. are supported by the intramural research program of the National Institutes of Health. We also acknowledge Jarrod Johnson, University of Utah for the technical support with the sequencing analysis. We declare that we have no conflict of interest with the content of this article.

Figures

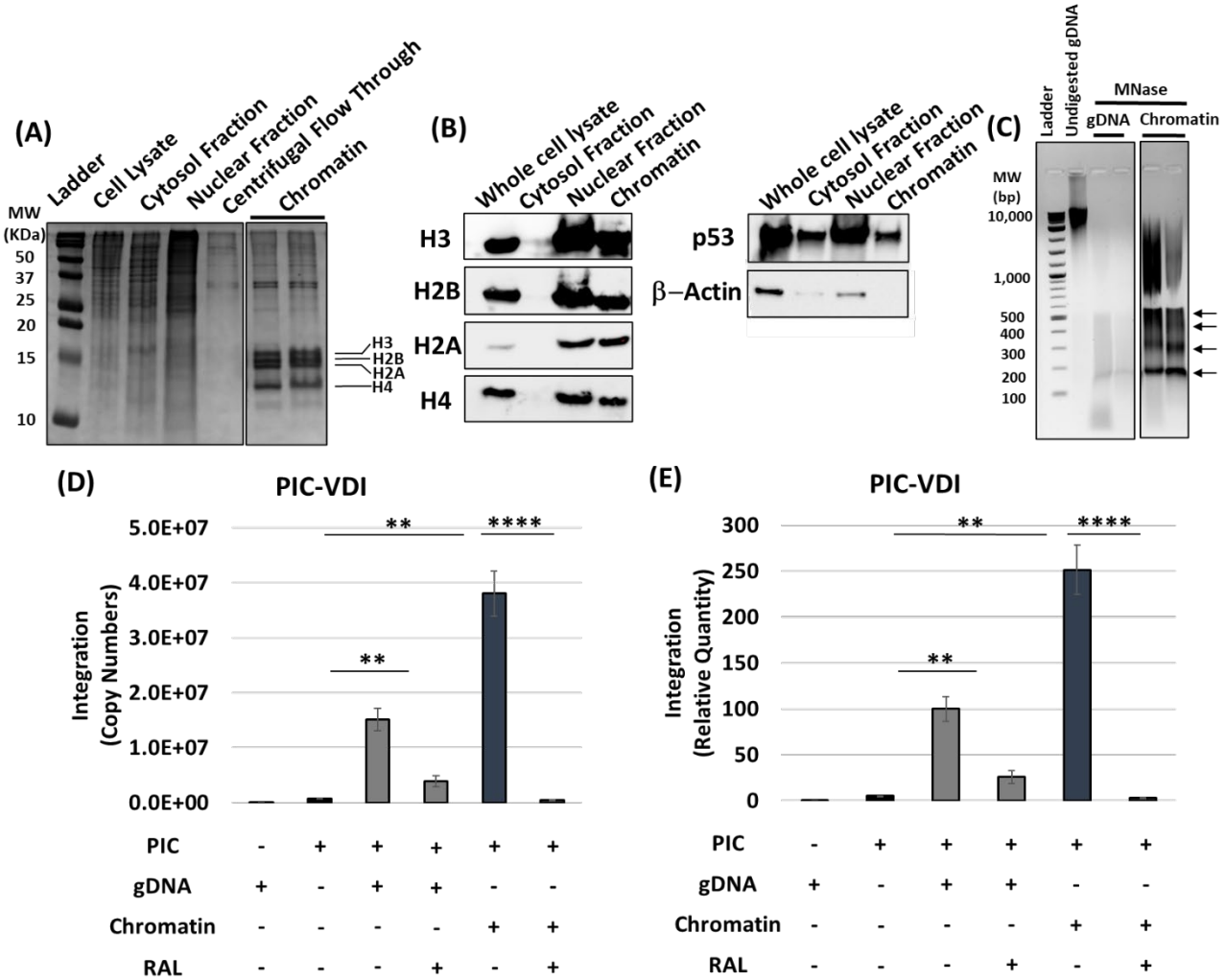

Figure 1. Chromatin is the preferred substrate for HIV-1 PIC-VDI. *Chromatin was isolated from HEK293T cells and assessed for the histone proteins and DNA. (A) Fractions from various steps of the chromatin preparation were analyzed by a 15% acrylamide gel, visualized by Coomassie staining. The chromatin fraction containing the canonical histone proteins: H3, H2B, H2A, and H4 are shown. (B) The histone proteins were detected by western blot in the whole cell lysate, cytosol fraction, nuclear fraction, and chromatin (left panel). Additionally, cytoplasmic, and nuclear proteins were probed in each fraction (right panel). (C) Protection of the chromatin DNA within nucleosomes was assessed by micrococcal nuclease (MNase) digestion. The arrows to the right of the gel indicative discrete DNA bands of nucleosome mediated protection. (D) HIV-1 PIC-VDI was measured by nested-PCR and represented as the copy numbers of integrated viral DNA, using 300 ng of chromatin and deproteinated genomic DNA as targets. As a negative control, 1 μM RAL-the integrase strand transfer inhibitor was used. (E) The copies of HIV-1 DNA integration were plotted relative to the integration into genomic DNA. The results in E are shown as the mean of viral DNA copy numbers of at least three replicates, with the error bars indicated the standard error mean (SEM). * Represents P > 0.05, ** P = 0.01 to 0.05, *** P = 0.01 to 0.001, P = 0.001 to 0.0001, and **** P < 0.0001.*

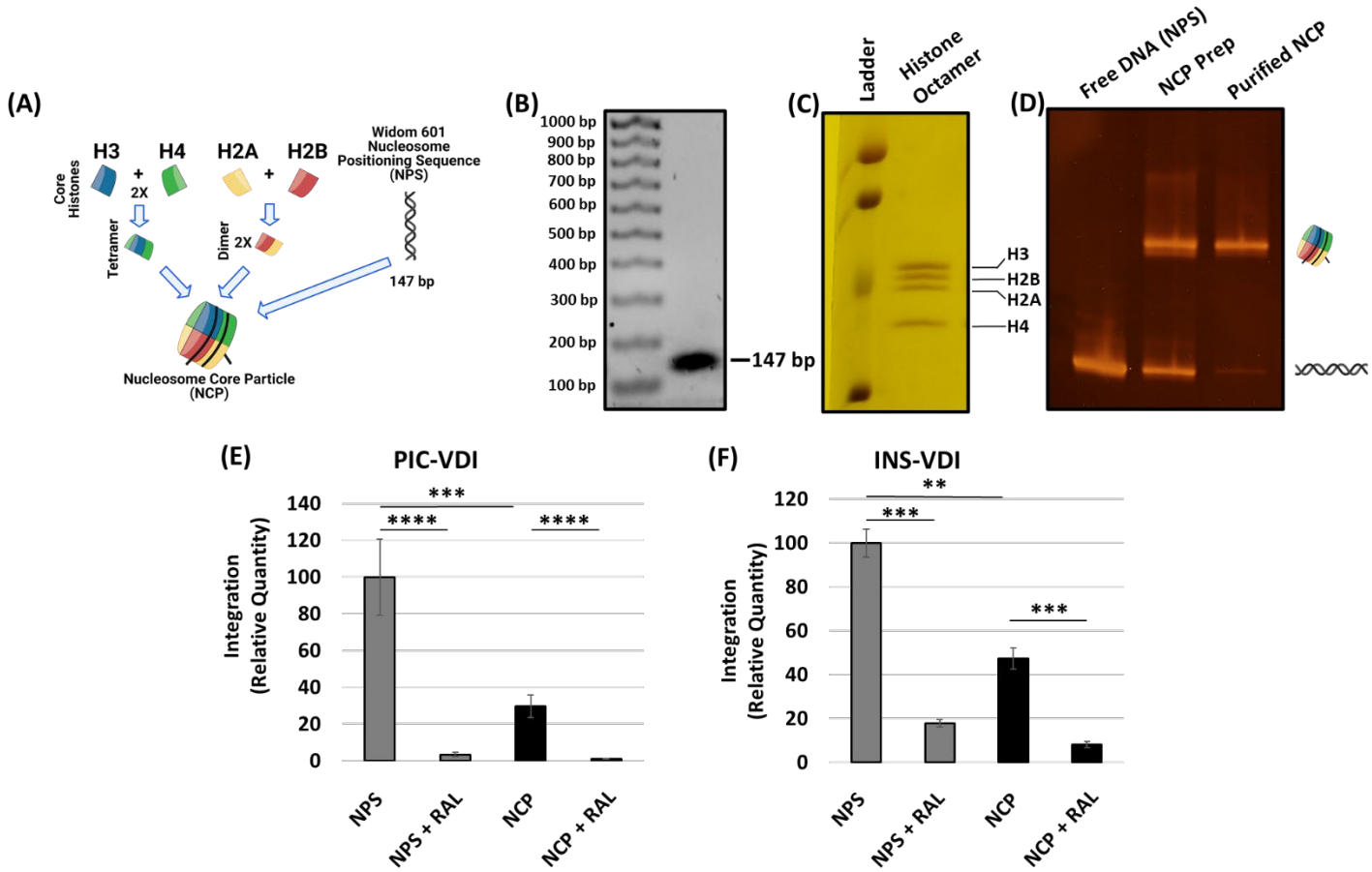

Figure 2. The NCP is a barrier to HIV-1 VDI. *(A) A schematic of the biochemical assembly of nucleosome core particle (NCP). The NCP is assembled with the Widom 601 nucleosome positioning sequence (NPS) and a recombinant human histone octamer. The histone octamer was assembled first by an equimolar addition of histone protein dimers H2A and H2B with the H3/H4 tetramer. (B) The 147 bp NPS DNA used for nucleosome assembly was analyzed on an 1.5% agarose gel and visualized by ethidium bromide staining. (C) The presence of individual histone proteins in the octameric histone assembly were visualized by SDS-AGE and Coomassie staining. (D) Biochemical assembly of the nucleosome was analyzed by an electro-mobility shift assay (EMSA). (E) PIC-VDI was assessed using 300 ng of the NPS and the NCP as targets, with 1 μM of RAL serving as a specific inhibitor for HIV-1 integration. (F) The intasome (INS) VDI was measured using quantitative PCR with the NPS and the NCP serving as targets. The data is represented as the relative quantity of VDI in reference to the NPS and error bars were generated from the SEM of at least three independent experiments. * Represents $P > 0.05$, ** $P = 0.01$ to 0.05, *** $P = 0.01$ to 0.001, $P = 0.001$ to 0.0001, and **** $P < 0.0001$.*

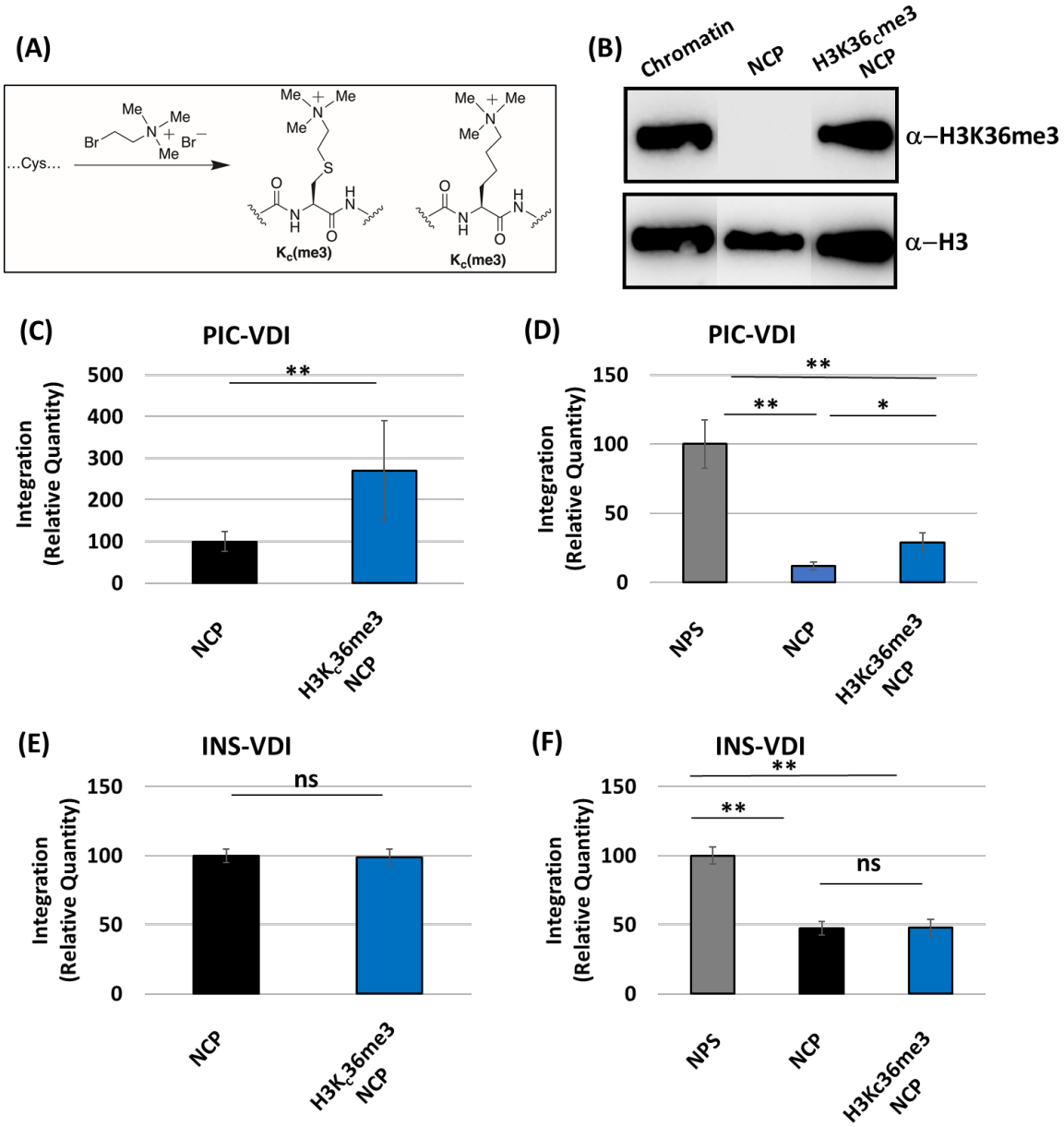

Figure 3. Nucleosomes containing trimethylated NCPs at Histone 3 Lysine 36 enhance PIC-VDI. *(A) A schematic illustrating the insertion of the H3K36me3 by site-directed mutagenesis of the K36 to cysteine (K36C). The K36C H3 undergoes alkylation to functionalize the K36C to create a biochemical mimic of the histone 3 trimethylation (H3K$_C$36me3). (B) Western blot analysis of the H3K36me3 and histone H3 in the H3K36$_C$me3-NCP compared to the unmodified NCP and the isolated chromatin. (C) PIC-VDI was measured with the NCP and the H3K36$_C$me3-NCP substrates. The integration data was plotted relative to the PIC-VDI into the NCP. (D) The PIC-VDI with the NPS, NCP and H3K36me3-NCP and the data was analyzed in reference to the NPS. (E) INS-VDI was measured comparing the NCP and H3K36me3-NCP. (F) Then the INS-VDI was assessed comparing the NPS, NCP and H3K36me3-NCP. The error bars were determined by the SEM of at least three independent replicates. * Represents P > 0.05, ** P = 0.01 to 0.05, *** P = 0.01 to 0.001, P = 0.001 to 0.0001, and **** P < 0.0001*

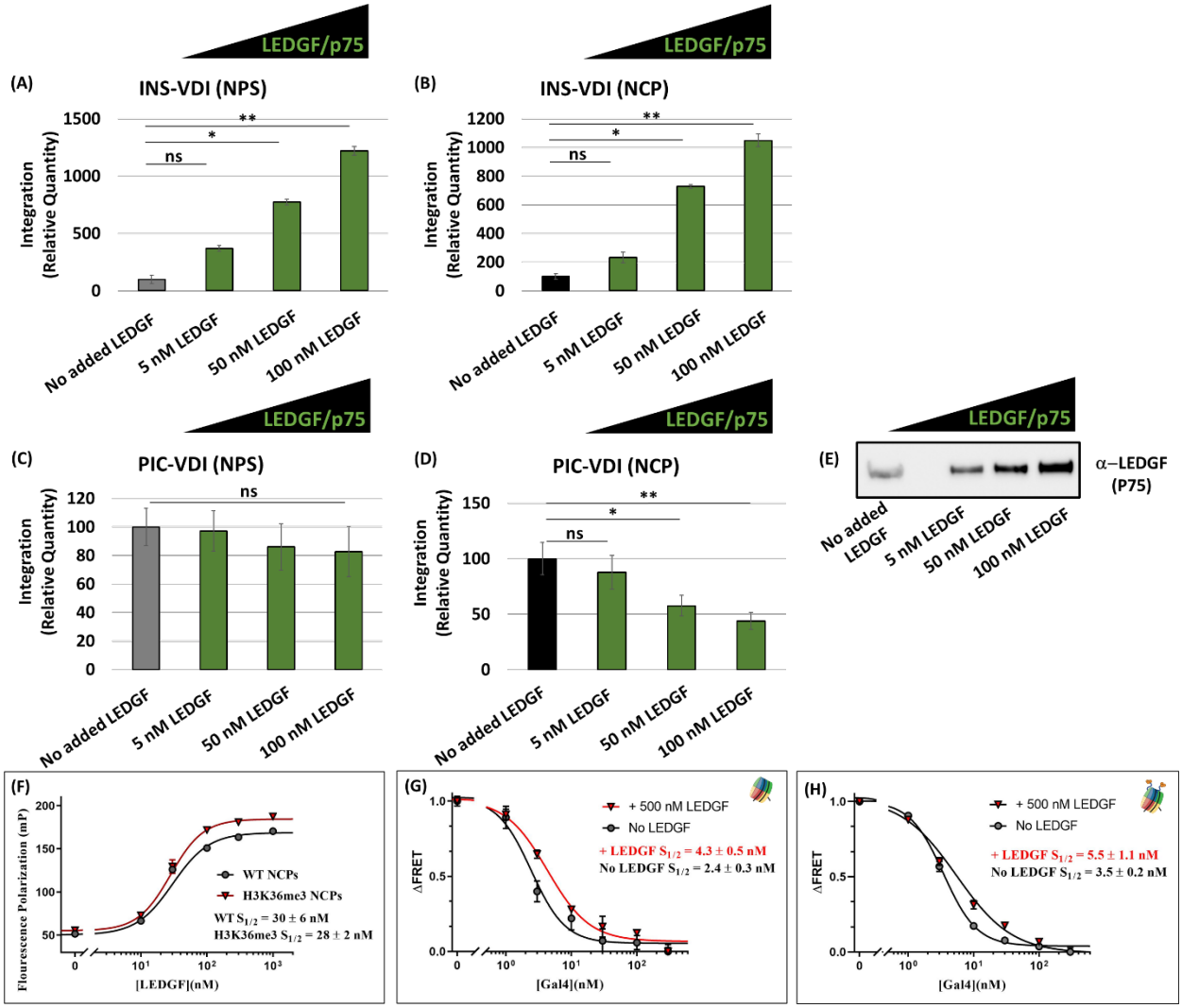

Figure 4. Presence of LEDGF/p75 stimulates INS-VDI but reduces PIC-VDI. *(A-B) INS-VDI [25 nM] was measured in the presence of the integration cofactor LEDGF/p75. LEDGF was added to the indicated reaction mixtures at 5, 10 and 25 nM to both the NPS substrate and the NCP substrate. (C-D) PIC-VDI was measured in the presence of LEDGF/p75 with both the NPS substrate and the NCP substrate. (E) Western blot analysis for LEDGF/p75 in the isolated PIC preparation and also in PICs supplemented with the recombinant LEDGF/p75 protein. (F) Fluorescence polarization assay were performed with fluoresceine labeled NCP to determine the LEDGF binding kinetics ($S_{1/2}$) to the nucleosomes. (G-H) The ensemble FRET measurements were detected by Cy3-Cy5 NCPs (Cy3 on the end of the NPS and Cy5 at the H2AK119C) and with titrations of GAL4 in the presence of LEDGF/P75 at saturating amounts of the unmodified NCP and H3K36$_C$me3-NCP. The error bars represent the SEM of at least three independent experiments. * Represents P > 0.05, ** P = 0.01 to 0.05, *** P = 0.01 to 0.001, P = 0.001 to 0.0001, and **** P < 0.0001.*

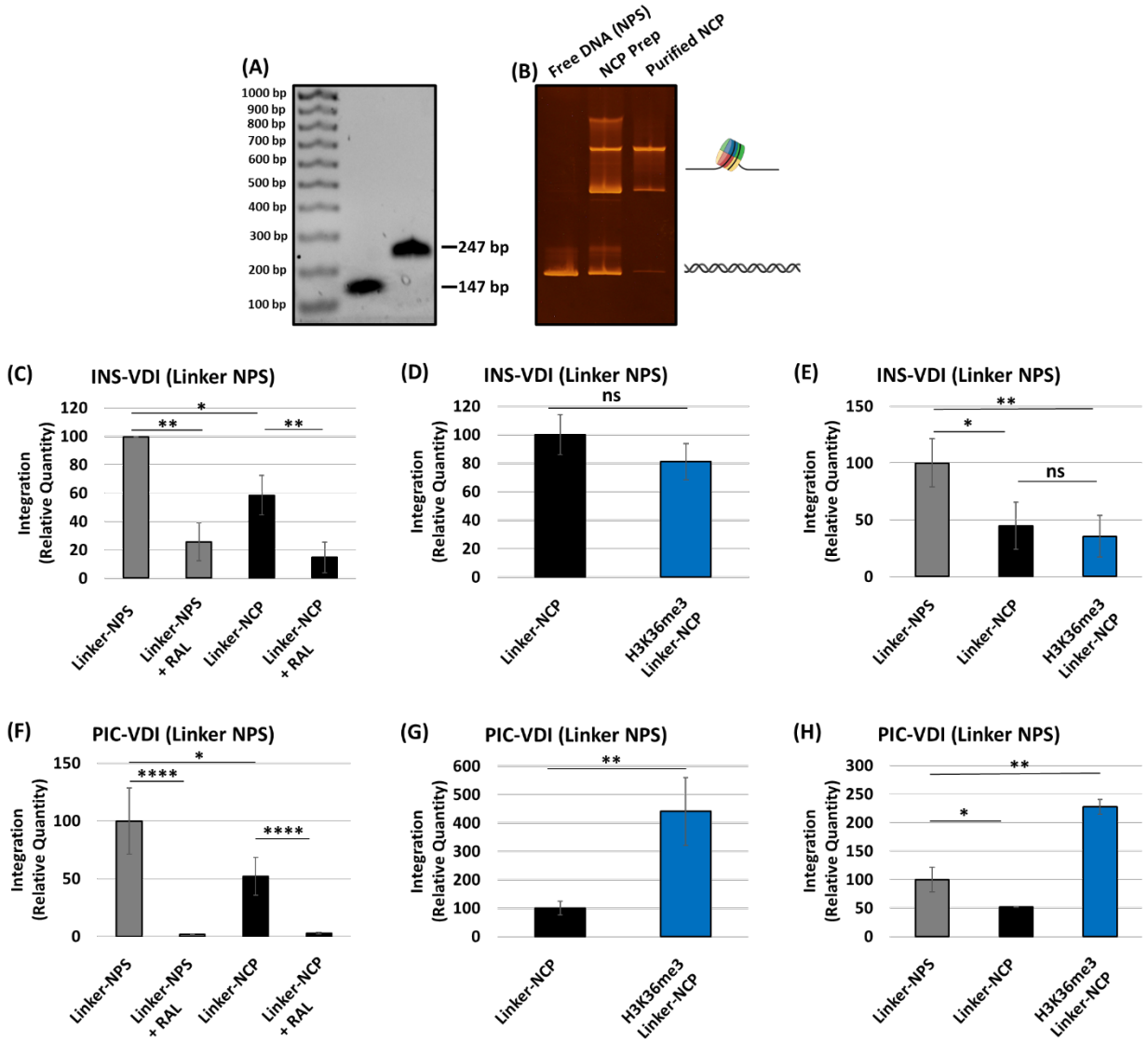

Figure 5. The NCP with linker DNA and the H3K36me3 is an optimal substrate for PIC-VDI. *The nucleosome containing 50 bp of linker DNA flanking the Widom 601 NPS (linker-NPS) was assembled, resulting in an NCP with linker substrate (linker-NCP) that is 247 bp. (A) The 147 bp and 247 bp NPS DNA was analyzed on an 1.5% agarose gel and visualized by ethidium bromide staining. (B) Biochemical assembly of nucleosome with the 247 bp NPS was analyzed by EMSA. (C) The relative quantity of INS-VDI was measured with the linker-NPS, compared to the linker-NCP. The integrase inhibitor, RAL, was included as a control for VDI. (D) The INS-VDI with linker-NCP in reference to the H3K36me3 NCP was plotted. (E) The linker-NPS, linker-NCP and linker-H3K36me3-NCP substrates were compared for INS-VDI relative to the linker-NPS. (F) PIC-VDI was assessed with the linker-NPS and linker-NCP substrates. (G) The linker-NCP and linker-H3K36me3-NCP were compared for the relative PIC-VDI. (H) The PIC-VDI was measured comparing the linker-NPS, to the linker-NCP and the linker-H3K36me3-NCP. All the results are shown as relative integration quantity and represent the mean of at least three independent experiments. Error bars represent the SEM and * Represents P > 0.05, ** P = 0.01 to 0.05, *** P = 0.01 to 0.001, P = 0.001 to 0.0001, and **** P < 0.0001.*

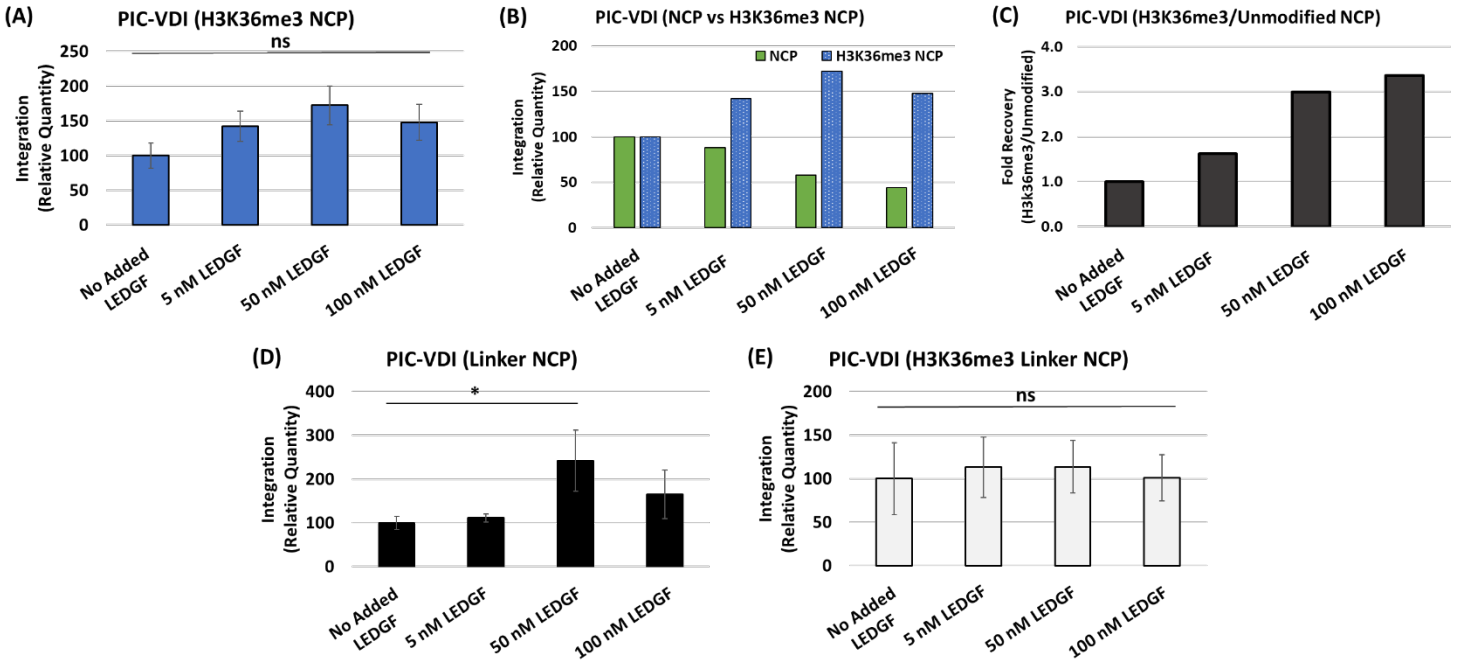

Figure 6. The H3K36me3-NCP and linker DNA support PIC-VDI in the presence of LEDGF/p75. *(A) PIC-mediated integration was measured using H3K36me3-nucleosomes as targets in the presence of LEDGF/p75 [5, 50 and 100 nM]. Integration data are presented relative the PIC reactions without added LEDGF/p75. (B) Comparative analysis of the relative PIC-VDI with the NCP and H3K36me3-NCP in the presence of LEDGF/p75. (C) The fold change was calculated between the unmodified NCP and H3K36me3-NCP effect on PIC-VDI in the presence of LEDGF/p75. (D) PIC-VDI was measured with LEDGF/p75 addition to the linker-NCP substrate. (E) PIC-VDI with the linker-H3K36me3-NCP in the presence of LEDGF/p75 is plotted relative to the assay without LEDGF/p75 supplementation. The error bars represent the SEM of at least three independent experiments and * Represents P > 0.05, ** P = 0.01 to 0.05, *** P = 0.01 to 0.001, P = 0.001 to 0.0001, and **** P < 0.0001.*

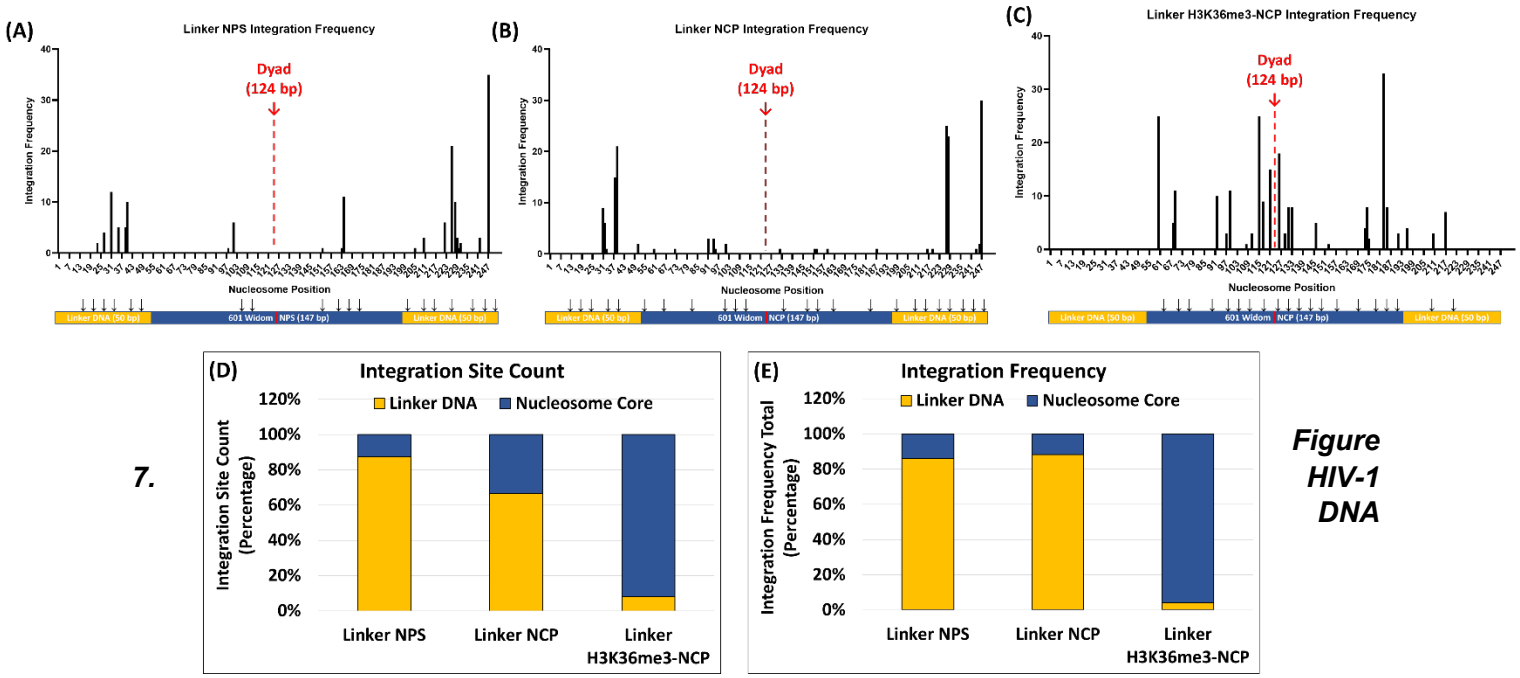

7. Figure HIV-1 DNA integration is preferentially directed into the core of the H3K36me3 containing nucleosomes. *To study HIV-1 integration preference, the DNA from the integration reactions were PCR amplified and subjected to next generation sequencing. The integration frequency within the linker substrates was determined by quantifying the integration junctions. The integration frequency is plotted as a histogram for (A) the linker-NPS, (B) linker-NCP, and (C) linker-H3K36me3-NCP substrates. (D) After quantifying the integration sites within the linker-substrates, the percentage of sites within the linker sequences and nucleosome core sequence were plotted for comparative analysis. (E) Then the frequency of integration junctions at a particular site within the sequence was determined. The integration frequency in the linker sequences and the nucleosome core sequence was quantified as a percentage of the total integration sites.*

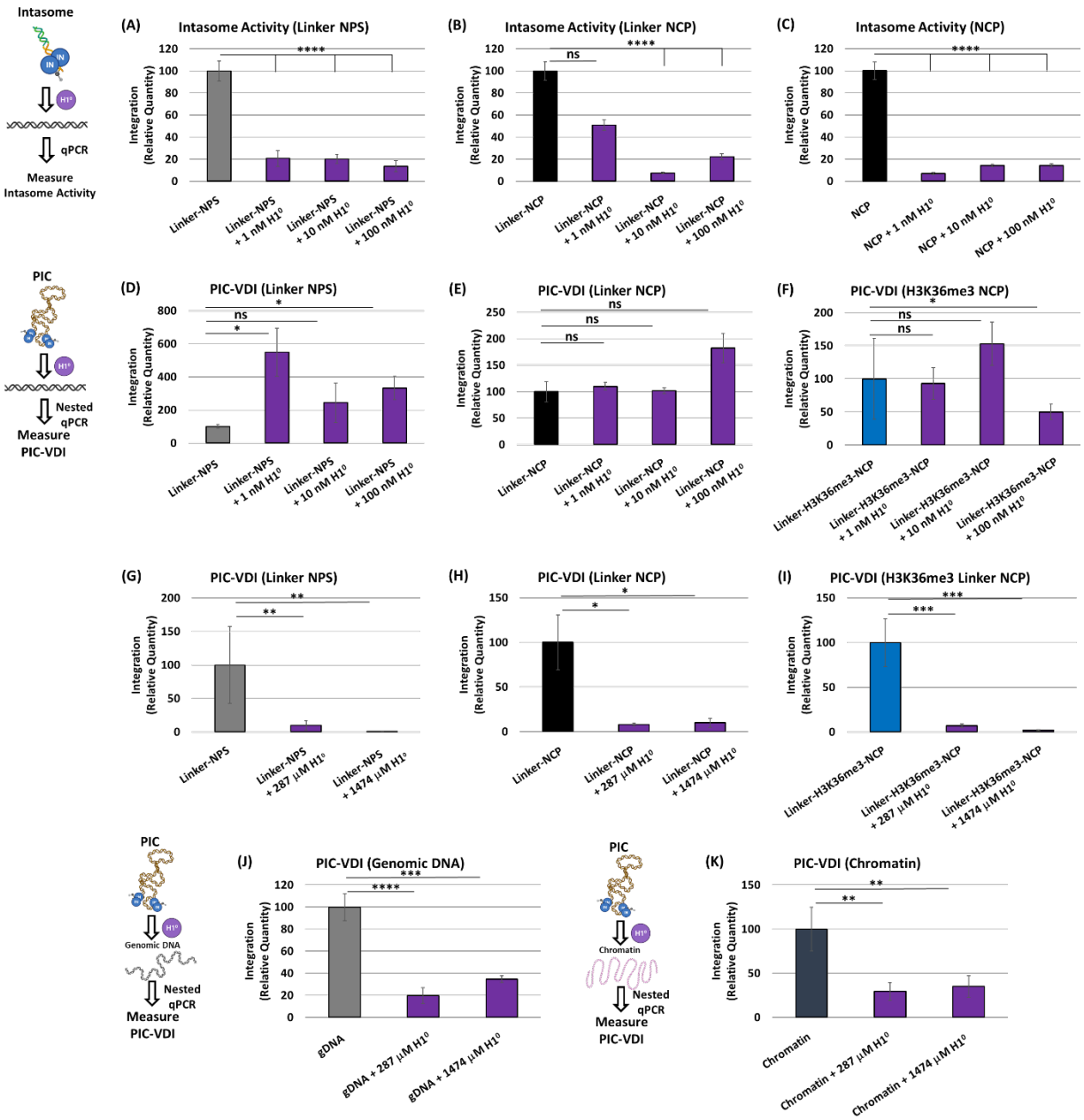

Figure 8. H1⁰ reduces HIV-1 DNA integration. *To probe the effects of H1 on HIV-1 integration, first INS-VDI [25 nM] was tested with (A) the linker-NPS, (B) the linker-NCP or (C) the NCP substrate preincubated with recombinant H1⁰ [1, 10 or 100 nM]. The results are the average relative quantity in reference to the assay lacking H1⁰ addition. Then, PIC-VDI was measured with (D) the linker-NPS, (E) the linker-NCP, (F) and the H3K36$_C$me3-linker-NCP substrates, that were preincubated with 1, 10 or 100 nM of H1⁰. (G-I) Next, either 287 or 1474 µM H1⁰ was added to the PIC-VDI measurements with the linker-NPS, the linker-NCP, and the H3K36$_C$me3-linker-NCP substrates. The µM concentrations of H1⁰ reflect amounts that are, respectively, 1:1 and 1:5 (w/w) stoichiometry of the substrate concentrations. The data shown is the relative quantity of the PIC integration relative to the assay lacking H1⁰ addition. The PIC-VDI was measured with (J) genomic DNA and (K) chromatin that were incubated on ice with 287 and 1474 µM of H1⁰. All data represent the mean of at least three independent experiments with the error bars representing SEM and * represents P > 0.05, ** P = 0.01 to 0.05, *** P = 0.01 to 0.001, P = 0.001 to 0.0001, and **** P < 0.0001.*

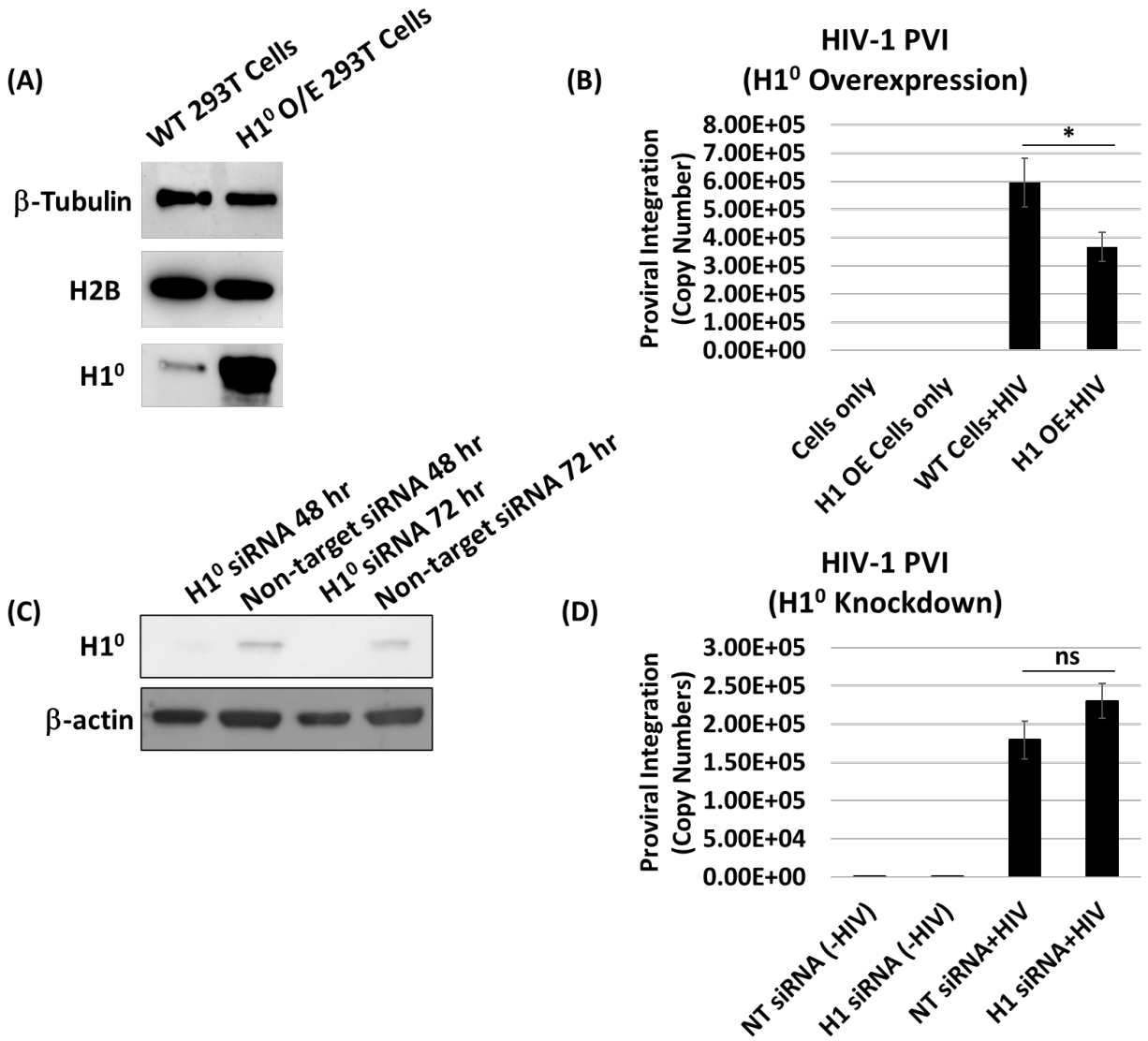

Figure 9. Histone H1 expression negatively regulates HIV-1 integration. *(A) Linker histone $H1^0$ was overexpressed in HEK 293T cells, and $H1^0$ protein was probed by western blot analysis, and the same blot was re-probed for β-tubulin and histone protein H2B as loading controls. (B) Proviral integration in the HEK 293T cells overexpressing $H1^0$. Cells were transfected with the pEV833 (GFP) expression construct for $H1^0$, then were inoculated with VSVG-Δenv-HIV-1 (GFP) particles. 24 h post inoculation, HIV-1 proviral DNA integration (PVI) was quantified by nested Alu-PCR. (C) In TZM-bl cells, $H1^0$ expression was depleted by siRNA targeting the $H1^0$ linker histone gene in parallel with a sequence scrambled non-target (NT) siRNA control. Western blot analysis confirms the depletion of $H1^0$ protein levels compared to scrambled siRNA control. The same blot was re-probed for β-actin. (D) The PVI of HIV-1 was measured in $H1^0$ expressing and $H1^0$ knockdown cells. All PVI data represent at least three independent experiments, and the error bars represent the SEM, * represents $P > 0.05$, ** $P = 0.01$ to 0.05, *** $P = 0.01$ to 0.001, $P = 0.001$ to 0.0001, and **** $P < 0.0001$.*

532 **Materials and Methods**

533 **Cell culture**

534 HEK293T and SupT1 cell lines were obtained from the American Type Culture Collection
535 (Manassas, VA). The TZM-bl reporter cell line was obtained from John C. Kappes, Xiaoyun Wu,
536 and Tranzyme, Inc., through the NIH AIDS Reagent Program, Division of AIDS, NIAID, NIH.
537 HEK293T and TZM-bl cells were cultured in Dulbecco modified Eagle medium (DMEM)
538 supplemented with 10% heat-inactivated fetal bovine serum (FBS), 2 mM glutamine, 1,000 U/ml
539 penicillin, and 100 mg/ml streptomycin. SupT1 cells were cultured in RPMI 1640 medium
540 supplemented with 10% heat inactivated FBS, 2 mM glutamine, 1,000 U/ml penicillin, and 100
541 mg/ml streptomycin. All cells were cultured at 37°C with 5% CO_2.

542 **Virus stocks**

543 High titer virus stocks were generated by transient transfection of HEK293T cells with the
544 HIV-1 plasmid construct pNL4-3 (NIH AIDS Reagents) by with polyethyleneimine (PEI). Briefly, 3
545 X 10^6 cells were seeded per 10-cm culture dish and cultured overnight. The following day, cells
546 in each dish were transfected using PEI and 10-15 μg of pNL4-3 DNA. At 16 hours post-
547 transfection, the cells were washed with phosphate buffered saline (1X PBS), replenished with 6
548 ml of DMEM. After 36 hours, the virus-containing culture supernatant of transfected cells were
549 harvested, cleared of debris by low-speed centrifugation, filtered through 0.45-mM filters, and
550 DNase I treated (Calbiochem; 20 μg/ml of supernatant) in the presence of 10 mM magnesium
551 chloride ($MgCl_2$) for 1 hour at 37°C. The virus infectivity was determined by using TZM-bl indicator
552 cells, as previously described [139].

553 **Chromatin isolation**

554 The chromatin isolation protocol is adapted from a published protocol [140]. HEK293T cells
555 were cultured to near confluency, then harvested and washed once with ice cold 1X PBS. Cells
556 were manually lysed on ice with a Dounce homogenizer (Wheaton) in *native lysis buffer* (NLB: 5
557 mM $MgCl_2$, 10 mM KCl, 20 mM HEPES pH 7.5, 250 mM sucrose, 0.5 mM dithiothreitol (DTT), 0.5
558 mM phenylmethanesulfonylfluoride (PMSF)) for 20 to 30 strokes. The lysate was washed and
559 homogenized with NLB twice by centrifugation at 4°C on 3,000x g for 15 minutes. After manual
560 lysis with NLB, the pellet was washed with modified buffer B (MBB: 5 mM $MgCl_2$, 10 mM KCl, 20
561 mM HEPES pH 7.5, 0.2 M ethylene glycol-bis(2-aminoethylether)- N, N, N', N'-tetra acetic acid
562 (EGTA), 0.5 mM DTT, 0.5 mM PMSF, and protease inhibitor cocktail (Promega, Madison, WI,
563 USA)). The resulting pellet was resuspended in 2 volumes of MBB, in reference to the pellet
564 volume, and then an equivalent volume of MBB/0.6 M KCl/ 10% glycerol was added in a dropwise
565 manner. The lysate was incubated at 4°C for 10 minutes with consistent rocking. After incubation,
566 the nuclear fraction was pelleted at a pre-cooled (4°C) centrifuge at maximum speed. The pelleted
567 nuclear fraction was resuspended in 20 times volume of medium salt buffer (MSB: 20 mM HEPES,
568 pH 7.5, 0.4 M NaCl, 1 mM ethylenediaminetetraacetic (EDTA), 5% glycerol (v/v), 0.5 mM DTT
569 and 0.5 mM PMSF) and manually homogenized. The nuclear pellet was centrifuged at 4°C for 10
570 minutes at 11,000x g, then resuspended in 4 pellet volumes of high salt buffer (HSB: 20 mM
571 HEPES, pH 7.5, 0.65 M NaCl, 1 mM EDTA, 0.34 M sucrose, 0.5 mM DTT and 0.5 mM PMSF).
572 Oligonucleosomes were released from the nuclear debris by manual homogenization on ice, and
573 fully separated from the debris by a maximum speed centrifugation at 4°C to collect the chromatin
574 containing supernatant. The chromatin was dialyzed for 16 hours against low salt buffer (LSB: 20

575 mM HEPES, pH 7.5, 0.1 M NaCl, 1 mM EDTA, 0.5 mM DTT and 0.5 mM PMSF). The dialyzed
576 chromatin was tested for nucleosome protection and the presence of histone proteins.

577 **Immunoblotting**

578 To detect proteins by immunoblot, samples were prepared in Radioimmunoprecipitation
579 assay (RIPA) buffer (Santa Cruz Biotechnologies Inc., Dallas, TX, USA) or the NLB buffer
580 supplemented with protease inhibitor cocktail and 10 μg/μL PMSF (Sigma-228 Aldrich, Saint
581 Louis, MO, USA) according to the standardized protocol. Protein concentrations were determined
582 using BCA (Bicinchoninic Acid) Protein Assay reagent (Thermo-Fisher Scientific, Waltham, MA,
583 USA) by the manufacturer's specifications. Equivalent amounts of protein from cellular lysates or
584 fractions were electrophoresed on pre-casted gels (Bio-Rad Laboratories, Hercules, CA, USA) or
585 in-house prepared 15% polyacrylamide gels and electrophoretically transferred to nitrocellulose
586 membranes using the Trans-Blot SD Semi-Dry Transfer Cell (Bio-Rad Laboratories, Hercules,
587 CA, USA). The membranes were incubated in blocking buffer [5% (w/v) nonfat milk in Tris-
588 buffered saline containing 0.05% Tween 20 (TBST); pH 8.0]. After blocking the membranes were
589 then probed with the indicated antibody diluted in blocking buffer; Abcam, Boston, MA, USA: H2A
590 (ab18255), H2B (ab1790), H3 (ab1791), H4 (ab7311), $H1^0$ (ab218417); Active Motif, Carlsbad,
591 CA, USA: H3K36me3 (ab_2615073); Bethyl Laboratories, Inc., Montgomery, TX, USA::
592 LEDGF/P75 (A300-848A); Cell Signaling Technology: p53 (2527S); Proteintech, Rosemont, IL,
593 USA: GAPDH (60004-1), and subsequently with secondary antibody conjugated to horseradish
594 peroxidase [anti-rabbit 1:10,000 (v/v); anti-mouse 1:10,000 (v/v)]. The membranes were washed
595 with 1X TBST buffer at least 3 times for 15 minutes each wash, and immunocomplexes were
596 detected by clarity enhanced chemiluminescence (ECL) method (Bio-Rad Laboratories, Hercules,
597 CA, USA).

598 **Isolation of preintegration complexes (PIC) from HIV-1 infected SupT-1 cells**

599 HIV-1 PICs were isolated from acutely HIV-1 infected T cells as described by
600 Balasubramaniam and colleagues [71-74]. Briefly, 8 X 10^7 of SupT1 cells were spinoculated (480 X
601 *g*) with DNase I-treated wild type virions for 2 hours at 25°C, and then cultured for 5 hours at 37°C.
602 The infected cells were then harvested by centrifugation (300 X *g*) for 10 minutes at room
603 temperature. The cell pellet was washed twice with 2 ml of buffer $K^{-/-}$ (20 mM HEPES, [pH 7.5],
604 150 mM potassium chloride (KCl), 5 mM $MgCl_2$). Subsequently, the cell pellet was gently
605 resuspended in 2 ml of ice-cold buffer $K^{+/+}$ (20 mM HEPES, [pH 7.5], 150 mM KCl, 5 mM $MgCl_2$,
606 1 mM dithiothreitol [DTT], 20 mg/ml aprotinin, 0.025% [wt/vol] digitonin). The cell suspension was
607 transferred to a chilled 2 ml microcentrifuge tube and incubated on a rocking platform (60 to 80
608 rocking motions/ minute) for 10 minutes at room temperature. The cell lysate was centrifuged
609 (1,500 X g) for 4 minutes at 4°C to separate the cytoplasmic and nuclear fractions. The
610 supernatant (cytoplasmic fraction) was transferred to a fresh 2 ml microcentrifuge tube and
611 centrifuged again (16,000 X g) for 1 minute at 4°C to clear residual nuclear debris. The resulting
612 cytoplasmic faction was treated with RNase A (Invitrogen, Waltham, MA, USA) at a final
613 concentration of 20 mg/ml and incubated for 30 minutes at room temperature. Finally, sucrose
614 (60% [wt/vol]) was added to a final concentration of 7% and the contents were thoroughly mixed.
615 Aliquots of the cytoplasmic fraction were flash-frozen in liquid nitrogen and stored at -80°C for
616 long-term storage. The cytoplasmic fraction aliquots were used as the source of HIV-1 PICs in
617 assays.

618 **Assay for measuring PIC-viral DNA integration (VDI)**

619 The *in vitro* integration assays were performed using a modified version of a protocol
620 detailed by Balasubramaniam and colleagues [72-74]. The *in vitro* integration reaction was carried
621 out by mixing 50 μl of PIC with 300 ng of the indicated target DNA, then allowing the mixture to
622 incubate at 37°C for 45 minutes. The integration reaction was stopped by adding SDS, EDTA,
623 and proteinase K to a final concentration of 0.5%, 8 mM, and 0.5 mg/ml, respectively, followed by
624 an overnight incubation at 55°C. The deproteinized reaction was brought to 200 μl and mixed with
625 an equal volume of phenol [pH 8.0] and thoroughly mixed by vortexing, and centrifuged (17,000
626 X g) for 2 minutes at room temperature. The aqueous phase is extracted once with an equal
627 volume of phenol-chloroform (1:1) mixture, followed by an equal volume of chloroform. The DNA
628 was precipitated by adding 2.5 volumes of 100% ice-cold ethanol in the presence of sodium
629 acetate (0.3 M, final concentration) and the coprecipitant glycogen (25 to 100 mg, final
630 concentration), followed by a minimum incubation for 2 hours at -80°C. The sample was
631 centrifuged at maximum speed for 30 minutes at 4°C, and the resultant DNA pellet was washed
632 once with 70% ethanol using maximum speed centrifugation for 15 minutes at 4°C. The
633 precipitated DNA was air dried at room temperature, resuspend in 50 μl of nuclease free water,
634 and used as the template DNA for the nested qPCR to measure PIC-mediated viral DNA
635 integration.

636 The nested PCR consists of two rounds of PCR to amplify the junction between the viral
637 DNA and target DNA, followed by a quantitative PCR (qPCR) specific to the viral DNA. A first-
638 round standard PCR, designed to amplify only the integrated virus-target DNA junctions, was
639 performed in a final volume of 50 μl containing 5 μl of purified DNA product from the integration
640 reaction, 500 nM concentration of each primer against the indicated target DNA (Table S2) and
641 the viral long terminal repeat (LTR) [5'-GTGCGCGCTTCAGCAAG- 3'], 1X Bestaq PCR buffer
642 (Applied Biological Materials Inc., Richmond, BC, Canada), dNTP nucleotide mix containing 200
643 mM concentrations of each nucleotide (Promega, Madison, WI, USA), and 1.25 U of Bestaq DNA
644 Polymerase (Applied Biological Materials Inc., Richmond, BC, Canada) with the following
645 thermocycling conditions: 95°C for 5 minutes, followed by 25 cycles at 95°C for 30 seconds, 55°C
646 for 30 seconds, and 72°C for 30 seconds (for the Widom 601 NPS DNA) or 2 minutes (for
647 chromatin or genomic DNA), and a final extension at 72°C for 10 minutes. The second-round
648 qPCR designed to amplify on the viral LTR-specific region contained one-tenth (5 μL) the volume
649 from the first-round PCR product as the template DNA, 1X iTaq Universal Probe Supermix (Bio-
650 Rad Laboratories, Hercules, CA, USA), 300 nM concentrations each of the viral LTR-specific
651 primers that target the R region (5'-TCTGGCTAACTAGGGAACCCA-3') and the U region (5'-
652 CTGACTAAAAGGGTCTGAGG-3'), and a 100 nM concentration of TaqMan probe (5'-6-
653 carboxyfluorescein[FAM]-TCAGCATTATCAGAAGGAGCCACC-6-carboxytetramethylrhodamine
654 [TAMRA]-3'). The qPCR run included an initial incubation at 95°C for 3 minutes, followed by 39
655 cycles of amplification and acquisition at 94°C for 15 seconds and 58°C for 30 seconds, and a
656 final incubation at 72°C for 30 seconds. During qPCR of the samples, a standard curve was
657 generated under the same conditions in parallel using 10-fold serial dilutions of known copy
658 numbers (10^0 to 10^8) of the HIV-1 molecular clone plasmid. Data were analyzed using CFX
659 Manager software (Bio-Rad Laboratories, Hercules, CA, USA), and integrated viral DNA copy
660 numbers were determined by plotting the qPCR data against the standard curve.

661 **Nucleosome positioning sequence DNA preparation**

662 The DNA molecules used for nucleosome assembly were generated by PCR from a
663 pUC19 clone containing the Widom 601 nucleosome positioning sequence (NPS). DNA products
664 from a 48-well PCR plate (50 - 100 μL reaction per well) were pooled and injected into an anion
665 exchange column (MonoQ-GL, GE Healthcare Life Sciences, Marlborough, MA, USA) for
666 purification. After extensive washing with 0.5X tris-EDTA (TE) buffer, the DNA was eluted with a
667 0 – 1.0 M NaCl linear gradient in 0.5X TE buffer, pH 7.5. The fractions containing the PCR product
668 was pooled and concentrated by a minimum cut-off of 10 MWCO spin column (Amico Ultra,
669 Millipore Sigma, Burlington, MA, USA) in 0.5X TE.

670 **Nucleosome Reconstitution**

671 Nucleosomes were made as previously described [77]. DNA was mixed with histone
672 octamer in a molar ratio of 1.25:1 in 0.5X TE pH 8, 2 M NaCl, and 1 mM benzamidine
673 hydrochloride and dialyzed via double dialysis into 0.5X TE pH 8 and 1 mM benzamidine
674 hydrochloride. Reconstituted nucleosomes were separated from free DNA using
675 ultracentrifugation with a 5 - 30% w/v sucrose gradient spun at 41,000 rpm for 22 hours. Gradients
676 were fractioned and ran on a 0.3X TBE, 5% acrylamide gel at 300 V for 1 hour to determine
677 nucleosome containing fractions. Selected fractions were concentrated, and buffer exchanged
678 into 0.5X TE pH 8.0 using centrifugal filters and final concentrated nucleosomes were run on
679 acrylamide gels as before to verify purity.

680 **Deposition of methyl-lysine analog on histone H3**

681 Human H3.2 (C110A, K36C) was created by site-directed mutagenesis using a Stratagene
682 QuickChange XL kit. The mutant histone was then expressed in *E. coli* BL21(DE3) pLysS cells
683 and purified as previously described [77]. The methyl-lysine analog was then deposited onto
684 H3.2(C110A, K36C) based on a previously reported protocol [87,141]. Initially, 5 mg of the mutant
685 histone was suspended in 980 μL of alkylation buffer (1 M HEPES pH 7.8, 4 M guanidine–HCl,
686 and 10 mM D/L-Methionine) and allowed to unfold for 1 hour. Then histones were reduced with
687 6.66 mM dithiothreitol for 1 hour at 37°C. After reducing, 100 mg of (2-bromoethyl)
688 trimethylammonium bromide was added to the histones. The reaction was then covered and
689 stirred for 5 hours at 50°C. The reaction was quenched with 50 μL of 14.3 M 2-mercaptoethanol.
690 Histones were then desalted using a PD 10 desalting column and dried via vacuum concentration.
691 Labeling efficiency was confirmed by MALDI-TOF mass spectrometry.

692 **HIV-1 Intasome (INS) preparation and assembly**

693 The HIV-1 intasomes used in our study were prepared by using published methods [81,82].
694 Briefly, a double-stranded preprocessed viral DNA substrate was used as the donor DNA
695 (Integrated DNA Technologies, Coralville, IA, USA). A 25-base oligonucleotide (5'-
696 AGCGTGGGCGGGAAAATCTCTAGCA-3') was synthesized with a complementary 27-base
697 oligonucleotide (5'-ACTGCTAGAGATTTTCCCGCCCACGCT-3') to provide the 3'-OH recessed
698 end for the preprocessed intasomes. The recombinant Sso7d-integrase (Sso7d-IN) was
699 expressed and purified in Escherichia coli BL21 (DE3), and the cells were lysed in buffer
700 containing 20mM HEPES (pH 7.5), 10% glycerol, 2mM β-mercaptoethanol (β-ME), 20mM
701 imidazole, and 1 M NaCl. The protein was purified by nickel affinity chromatography and
702 subsequently by gel filtration on a Hi load 26/60 Superdex-200 column (GE Healthcare,
703 Milwaukee, WI, USA) equilibrated with 20mM HEPES (pH 7.5), 10% glycerol, 2mM DTT, and

704 500mM NaCl. The protein was concentrated using an Amicon centrifugal concentrator (EMD
705 Millipore, Burlington, MA, USA) and then used for intasome assembly or flash frozen in liquid
706 nitrogen and stored at -80°C. Intasomes were assembled by incubating 3 mM HIV-1 integrase
707 and 1 mM 3'-processed or unprocessed viral DNA substrate in 20mM HEPES (pH 7.5), 20%
708 glycerol, 5mM 2-mercaptoethanol, 5mM $CaCl_2$, 2mM $ZnCl_2$, 100mM NaCl, and 50mM 3-
709 (benzyldimethylammonio) propanesulfonate (NDSB-256) at 30°C for 1 h. Assembled intasomes
710 were purified as described previously [81,82], aliquoted, flash frozen in liquid nitrogen, and stored at
711 -80°C.

712 **Assay to measure HIV-1 Intasome-VDI**

713 Intasome viral DNA integration (INS-VDI) assays were assembled on ice with 25 nM INS
714 in 20 mM HEPES pH 7.5, 20% glycerol, 10 mM DTT, 5 mM $MgCl_2$, 4 mM $ZnCl_2$ and 100 mM NaCl
715 in a 20 μl reaction volume. *In vitro* integration reaction with intasomes were carried out with 300
716 ng of target DNA, the incubated at 37ºC for 1 hour. The reaction was terminated with 0.5% SDS
717 and 8 mM EDTA, together with 0.5 mg/ml protease K and deproteinated for 1 hour at 55ºC. The
718 DNA was recovered by ethanol precipitation, as described above, and resuspend in the original
719 reaction volume of nuclease-free dH_2O. The recovered DNA was used as the template DNA for
720 a SYBR green-based quantitative PCR to amplify the junctions between viral DNA substrate and
721 the target DNA for the indicated assay. The qPCR reaction was carried out in a 20 μl volume,
722 containing 1 to 2 μl (5 - 10 ng) of purified DNA product from the INS-VDI assay, 300 nM
723 concentration of each primer targeting the viral DNA substrate (5'-
724 AGCGTGGGCGGGAAAATCTC-3') and the indicated target DNA (table 1) and 1X i*Taq* Universal
725 SYBR Green Supermix (Bio-Rad Laboratories, Hercules, CA, USA). The qPCR cycling conditions
726 for quantifying INS activity included an initial incubation at 95ºC for 3 minutes, followed by 39
727 cycles of amplification and acquisition at 94ºC for 15 seconds, 55ºC for 30 seconds and 72ºC for
728 30 seconds. The thermal profile for melting-curve analysis was obtained by holding the reaction
729 at 65ºC for 30 seconds, followed by a linear ramp in temperature from 65 to 95ºC at a ramp rate
730 of 0.5ºC/second and acquisition at 0.5ºC intervals. The Maestro CFX program was used for data
731 analysis.

732 **FRET Titrations**

733 FRET efficiency measurements were carried out with a Horiba Scientific Fluoromax 4
734 Spectrofluorometer. Samples were excited at 510 and 610 nm and the photoluminescence
735 spectra were measured from 530 to 750 nm and 630 to 750 nm for donor and acceptor excitations,
736 respectively. FRET efficiencies from measured spectra were computed through the (ratio) A
737 method [142] using an in-house Matlab program. FRET efficiencies were then normalized as change
738 in FRET and fit to a binding isotherm using GraphPad 9.1.2 to determine $S_{1/2}$'s, the concentration
739 at which 50% of the nucleosome is bound by LEDGF/p75.

740 Titrations used a 60 μL reaction volume with 1 nM nucleosomes mixed into increasing
741 concentrations of GAL4. Each titration was repeated in the presence or absence of binding
742 saturation concentrations of LEDGF (500 nM). The conditions in each reaction were 75 mM NaCl,
743 10 mM Tris-HCl pH 8, 0.25% Tween20, and 10% glycerol. Titrations were repeated in triplicate to
744 acquire standard deviation errors.

745 **Fluorescence polarization**

746 Fluorescence polarization measurements were acquired with a Tecan infinite M1000Pro
747 plate reader by exciting samples at 470 nm and then measuring polarized emission at 519 nm
748 with 5 nm excitation and emission bandwidths. Fluorescence polarization of each sample was
749 calculated from:

750 $$P = \frac{I_{||} - I_{\perp}}{I_{||} + I_{\perp}}$$

751 where $I_{||}$ and $I_{\perp}$ is the emission polarized parallel and perpendicular to the polarized excitation
752 light, respectively. The data was then fit to a binding isotherm using GraphPad 9.1.2 to determine
753 $S_{1/2}$'s.

754 Titrations used a 30 µL reaction volume with 5 nM nucleosomes mixed into increasing
755 concentrations of LEDGF. The conditions in each reaction were 75 mM NaCl, 15 mM Tris-HCl pH
756 7.5, 0.00625% Tween 20, and 3 mM dithiothreitol. The samples were loaded into a Corning round
757 bottom polystyrene plate and allowed to incubate at 4°C for 30 mins before measurements were
758 taken. Titrations were repeated in triplicate to acquire standard deviation errors.

759 **Proviral Integration (PVI) Assay**

760 Infection experiments were carried out by inoculating cells with psuedotyped HIV-1
761 particles (ref). HEK293T or TZM-bl (3.0 x 10^5 cells per well) were seeded in 6-well plates, cultured
762 overnight, and then washed with fresh medium. Virus stocks prepared in DMEM containing
763 Polybrene (6 µg/ml) and either 1 µM RAL, or 5 µM EFV were indicated were added to the cells.
764 The cells were then cultured for 24 to 48 hours at 37°C with 5% CO_2 and harvested for further
765 use. Total DNA from the infected and uninfected control cells was isolated using a Quick-DNA
766 miniprep kit according to the manufacturer-recommended protocol (Zymo Research, Irvine, CA,
767 USA). To measure HIV-1 PVI, a nested PCR method was used that consisted of a first-round
768 endpoint PCR with primers designed to amplify only the integration junctions between human *Alu*
769 repeats and HIV-1 viral DNA, followed by a second-round of qPCR with primers designed to
770 specifically amplify only the viral LTR from the first-round PCR products (ref). The first-round PCR
771 contained 100 ng of total DNA, 1X Bestaq PCR buffer (Applied Biological Materials Inc.,
772 Richmond, BC, Canada), dNTP mix containing 200 mM concentrations of each nucleotide
773 (Promega, Madison, WI, USA), 500 nM primers targeting *Alu* repeat sequence (5'-
774 GCCTCCCAAAGTGCTGGGATTACAG-3') and the HIV-1 Gag sequence (5'-
775 GTTCCTGCTATGTCACTTCC-3'), and 1.25 U of Bestaq DNA polymerase in a 50-µl final volume.
776 The first-round PCR conditions consisted of the following cycles: 95° C for 5 minutes, followed by
777 25 cycles of amplification at 94°C for 30 s, 50°C for 30 s, and 72°C for 4 min, and a final incubation
778 at 72°C for 10 min. The second-round PCR reaction consisted of one-tenth (5 µL) of the product
779 from the first-round PCR as the DNA template, 1X i*Taq* universal probe Supermix (Bio-
780 Laboratories, Hercules, CA, USA), 300 nM each of the viral Gag specific primers (F2: 5'-
781 TCAGCCCAGAAGTAATAC-3') and (R2: 5'-CACTGGATGCAATCTATC-3'), and 100 nM of the
782 TaqMan probe (5'-6-[FAM]- TCAGCATTATCAGAAGGAGCCACC-6-[TAMRA]-3'). The qPCR
783 program consisted of the following amplification conditions: 95° C for 3 min, followed by 39 cycles
784 of amplification and acquisition at 94°C for 15 s, 58°C for 30 s, and 72°C for 30 s. Concurrent with
785 the qPCR of the samples, a standard curve was generated in parallel and under the same

786 conditions using a 10-fold serial dilution of known copy numbers (1 X 10^0 to 1 X 10^8) of the HIV-1
787 molecular clone plasmid (NL4-3). The qPCR experiments were performed in triplicates, and the
788 data were analyzed using CFX Maestro software (Bio-Rad Laboratories, Hercules, CA, USA).
789 The integrated viral DNA copy numbers were calculated by plotting the qPCR data against the
790 standard curve.

791 **Sequencing Analysis of the integration junctions**

792 The first-round end point PCR product of the PIC-VDI assay was subjected to a second
793 end point PCR amplification with the same primers to increase the yield of DNA. The second
794 endpoint PCR amplification was subjected to a PCR DNA purification kit (Zymo Research) and
795 the DNA was submitted for sequencing as described by Christensen and colleagues, and
796 performed at the DNA Sequencing Core Facility, University of Utah [79]. In brief, 100 ng samples
797 were prepared using an Illumina TruSeq DNA PCR-Free Library Prep, fragmented to a mean size
798 of 200-250 bp, and sequenced on a NovaSeq Reagent Kit v1.5_150x150 flow cell, with a target
799 read depth of 5M reads per sample. Due to the relatively short target DNA length (247 bp) and
800 the viral DNA primer binding 84 bp upstream of the LTR (~720 bp into the HIV-1 genome)
801 generating a maximum integration junction less than 1Kb, sequencing the integration junctions
802 presented inherent technical limitations. This sequencing protocol was optimized for samples
803 larger than 1Kb, thus there were technical challenges for generating the expected thousands to
804 hundreds of thousands of reads with our samples. As a result, we selected the samples that
805 contained at the most contiguous integration junction reads for analysis. Therefore, two samples
806 per NPS-DNA, unmodified-NCP, and H3K36me3-NCP, that met these criteria were analyzed.
807 Next, fastq files were then filtered using SEAL to find reads that contained a 20 base kmer that
808 mapped to the end of the 5' LTR with at least 17/20 matches. These reads passing this filter were
809 then mapped onto the nucleosome target sequences to generate sam and bam files. The
810 Integrated Genomics Viewer (IGV) https://software.broadinstitute.org/software/igv/ was used to
811 visualize the integration junctions [143]. The integration junctions were tabulated by quantifying the
812 continuous junction between the target DNA (in grey) and the viral DNA sequence (red, green,
813 yellow, or blue), then plotted in excel.

Supplemental Figures

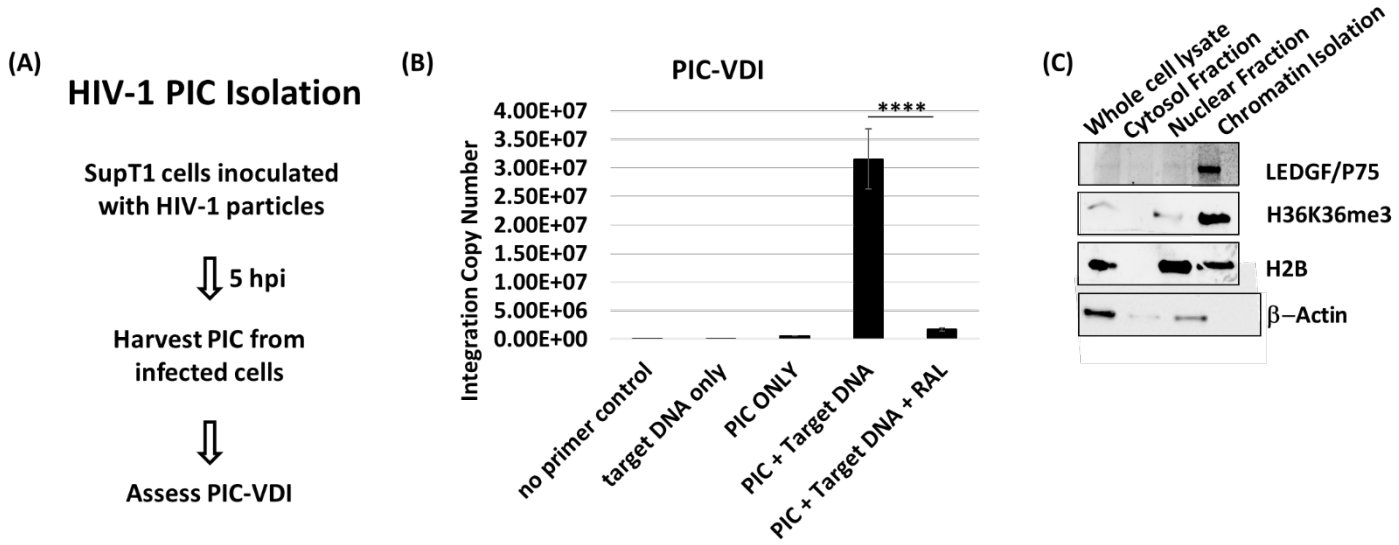

Supplemental Figure 1. Virus infectivity and HIV-1 PIC isolation. *(A) The isolation of HIV-1 PICs is shown as a diagram. First, HIV-1 virions were produced by transfecting HEK293T cells with the pNL4.3 HIV-1 molecular clone, collecting the supernatant 36-48 hours later, filtering the supernatant and treating with DNase I. Then HIV-1 pre-integration complexes (PIC) were isolated from SupT1 cells acutely infected with high tiger HIV-1 virions. The resultant PICs are assessed for viral DNA integration (VDI) using a nest-PCR assay. (B) HIV-1 PIC-VDI is measured by a nested PCR strategy that amplifies the DNA junction formed between the viral DNA and targeted substrate by the stand transfer activity of the HIV-1 integrase. The PIC-VDI is specifically inhibited by the integrase strand-transfer inhibitor raltegravir (RAL). The error bars were determined by the SEM and **** represents P < 0.0001. (C) The chromatin sample that was used as a substrate for PIC-VDI was probed by western blot analysis for the nuclear proteins associated with HIV-1 integration and cytoplasmic proteins.*

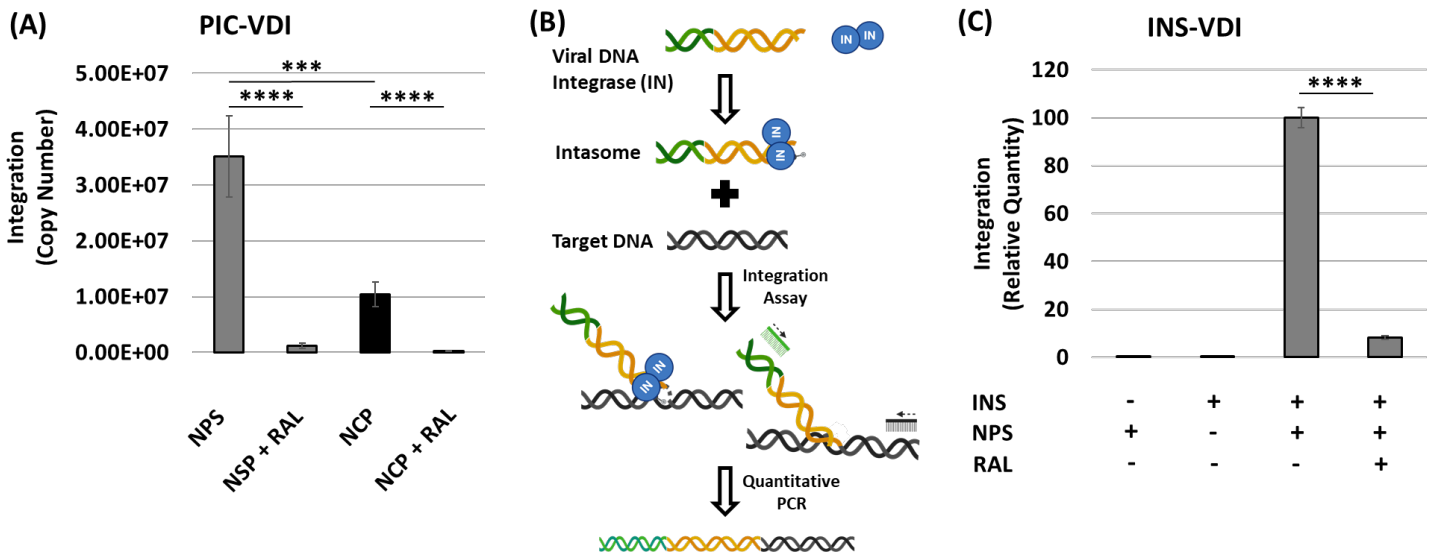

Supplemental Figure 2. The recombinant NCP is a barrier to PIC-VDI and INS-VDI. *(A) PIC-VDI was measured with the nucleosome positioning sequence (NPS) substrate and the nucleosome core particle (NCP) substrate, including RAL controls. The data is shown as the mean copy numbers of at least three independent PIC-VDI experiments. (B) A schematic of the intasome (INS) assembly. The INS was pre-assembled with the purified integrase protein and viral DNA sequences from the HIV-1 long-terminal repeat (LTR). Once assembled, the INS can carry out a DNA strand transfer reaction with any given target DNA. The INS-VDI is measured by quantitative PCR using primers designed for the INS donor DNA and the target DNA (acceptor DNA). (C) The INS-VDI was measured by qPCR with the NPS alongside the INS alone, substrate alone, or in the presence of the integrase inhibitor RAL. The error bars were determined by the SEM, and the *** represents P = 0.001 to 0.0001, **** P < 0.0001.*

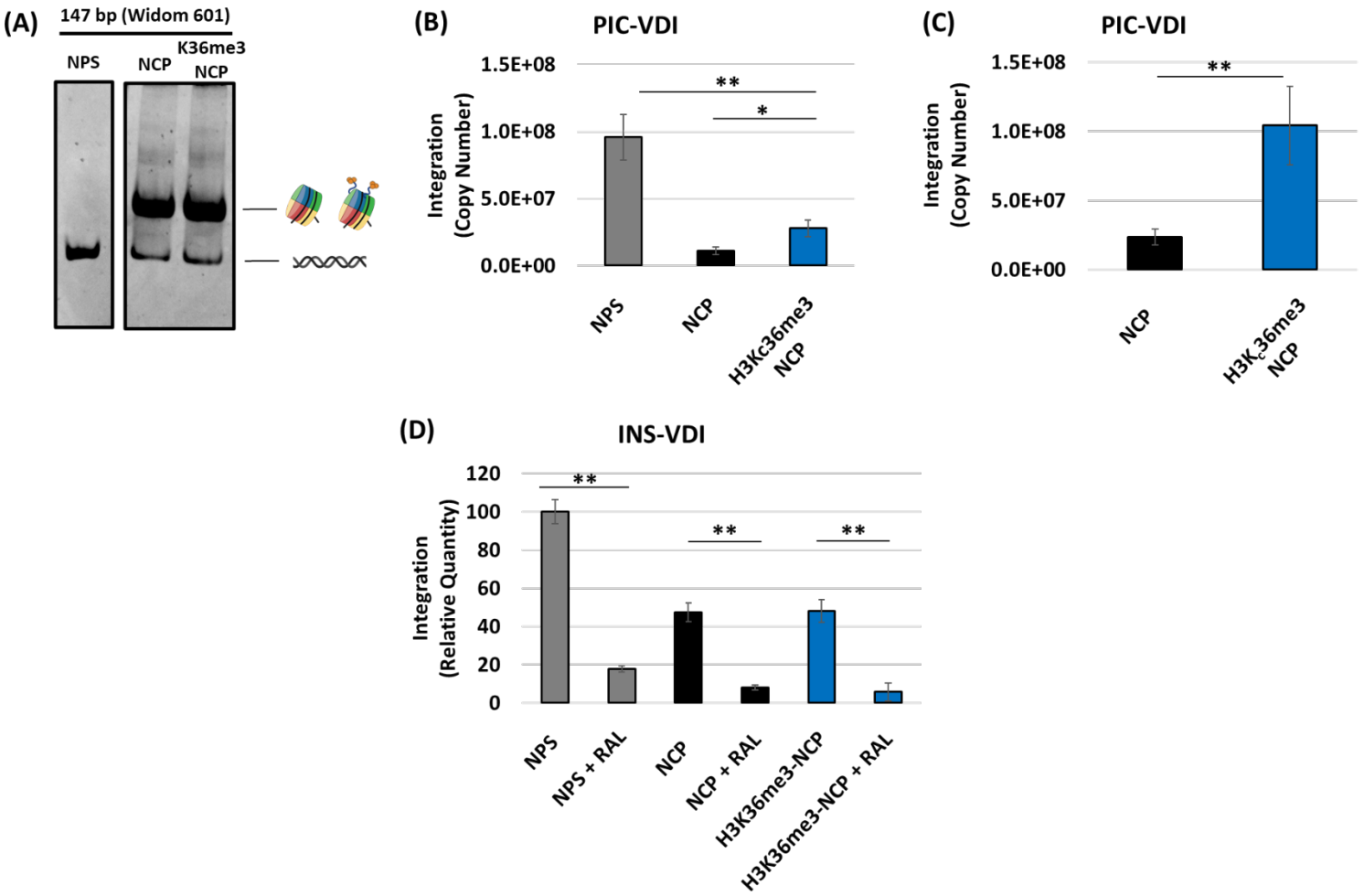

Supplemental Figure 3. Comparative analysis of the PIC-VDI and INS-VDI with the NPS, NCP and H3K36me3-NCP. *(A) The biochemically assembled NPS, NCP and H3K36$_C$me3-NCP were assessed by a 5% polyacrylamide gel electrophoresis (PAGE) and visualized with ethidium bromide staining. (B) Comparative analysis of the PIC-VDI with the NPS, NCP and H3K36me3-NCP was measured by nested qPCR, and the data is represented by the mean of viral DNA copy numbers from at least three independent experiments. (C) A direct comparison of the PIC-VDI with the NCP and H3K36me3-NCP is shown as the mean of copy numbers from independent experiments. (D) The INS-VDI was measured with the NPS, NCP and H3K36me3-NCP, including RAL controls. The error bars represent the SEM. * Represents P > 0.05 and ** P = 0.01 to 0.05.*

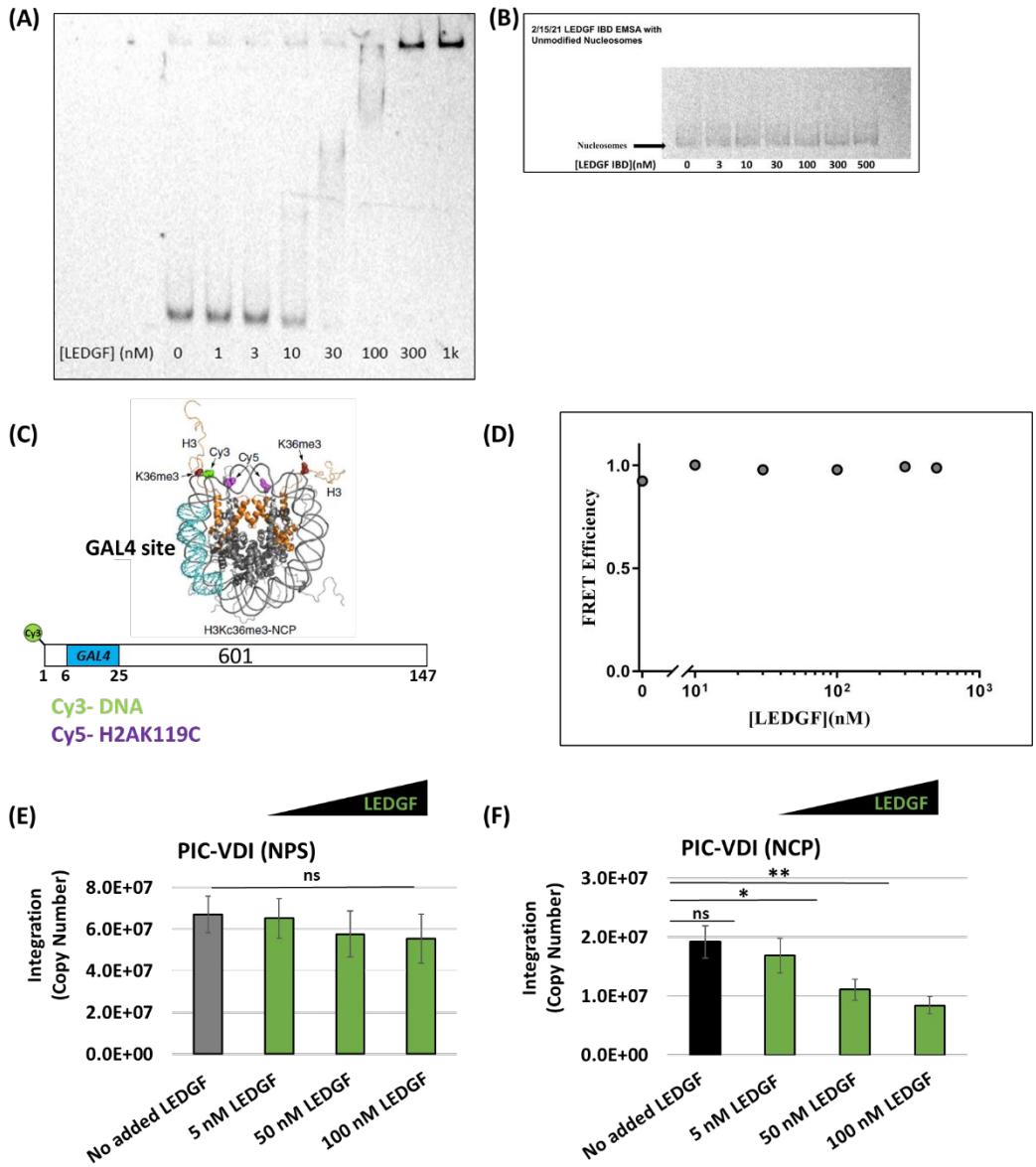

Supplemental Figure 4. LEDGF/p75 binds the NCP and specifically reduces PIC-VDI with the NCP. *(A) A schematic of the modified NCP for the FRET based binding assay is depicted. The ensemble FRET binding assay used NCPs labeled with Cy3 at the end of the NPS and a Cy5 at the H2AK119C position. A binding site for the transcription factor GAL4 was cloned into the NPS near the H3 tail protrusion site thru the nucleosomal DNA (6-25 bp) was designed to specifically determine the effect of LEDGF/p75 binding to the NCP. (B) The interaction between the NCP and LEDGF/p75 was assessed by EMSA. (C) Binding of the truncated mutant of LEDGF/p75, amino acids 341–429, that only contains the integrase binding domain (IBD) to the NCP was assessed for by EMSA. This truncated LEDGF/p75 lacks the AT-hook motifs nor the PWWP domain. (D) The FRET efficiency was measured in the presence of increasing amounts of LEDGF/p75. (E-F) The PIC-VDI with the NPS and the NCP were measured in the presence of LEDGF/p75 addition. These data are represented as the mean copy numbers of at least three independent experiments and the error bars represent the SEM. * Represents P > 0.05, ** P = 0.01 to 0.05, *** P = 0.01 to 0.001, P = 0.001 to 0.0001, and **** P < 0.0001.*

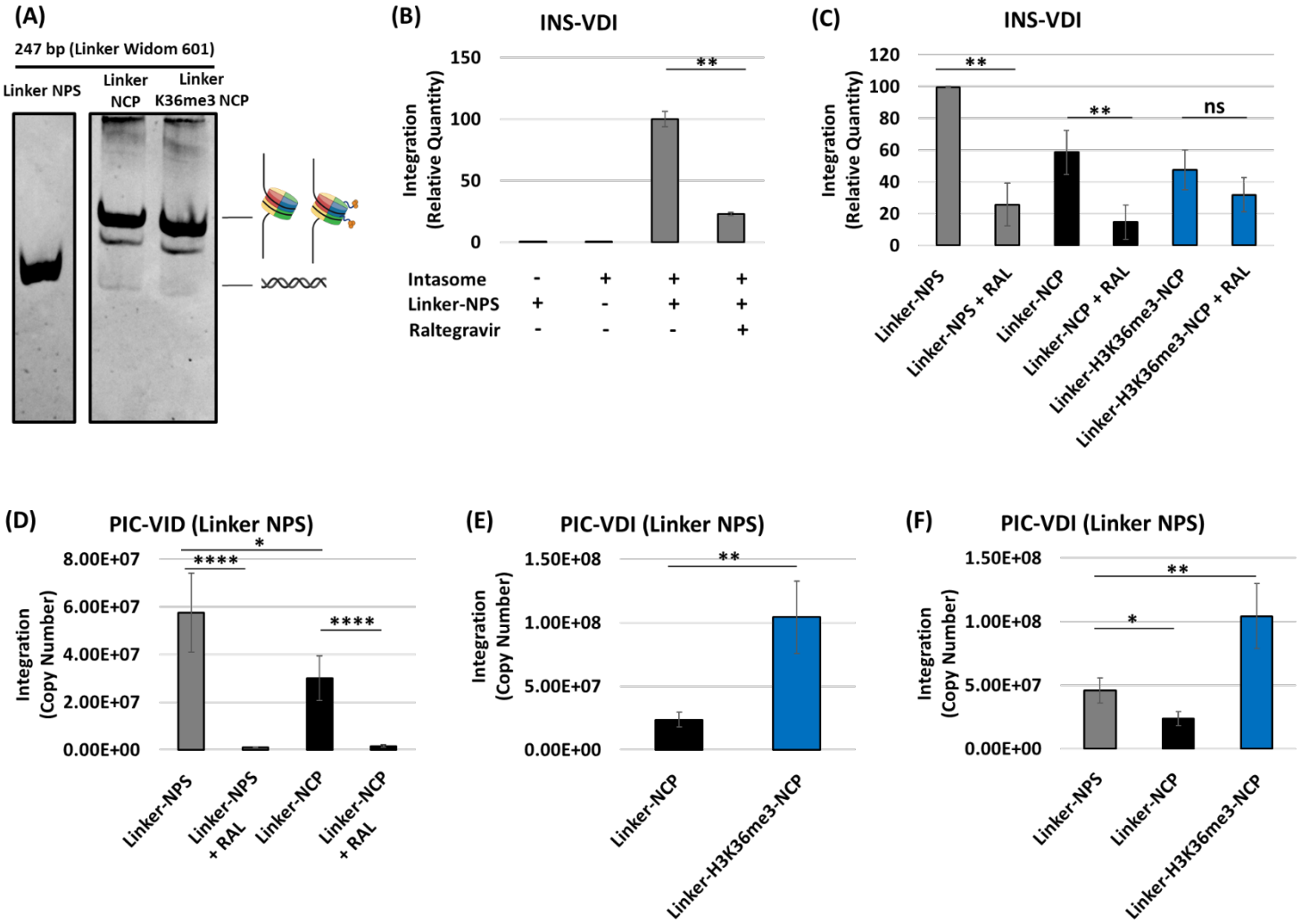

Supplemental Figure 5. The linker-H3K36me3-NCP is an optimal substrate for PIC-VDI, despite the linker-NCP remaining a barrier to HIV-1 VDI. *(A) The linker-NPS, linker-NCP, and linker-H3K$_C$36me3-NCP were assessed by PAGE. (B) The INS-VDI was measured with the linker NPS, compared to the intasome only, target DNA only and RAL integrase inhibitor control. (C) The NPS, NCP and H3K36me3-NCP linker substrates were tested for INS-VDI along with RAL control assays. (D) The PIC-VDI was measured with the linker-NPS and linker-NCP substrate alongside RAL control assays. (E) The PIC-VDI was measured comparing the linker-NPS, to the linker-NCP and the linker-H3K36me3-NCP. (F) The linker-NPS, linker-NCP and linker-H3K36me3-NCP were compared as substrates for PIC-VDI. These results are shown as the mean copy numbers of at least three independent VDI experiments and the error bars represent the SEM. * Represents P > 0.05, ** P = 0.01 to 0.05, *** P = 0.01 to 0.001, P = 0.001 to 0.0001, and **** P < 0.0001.*

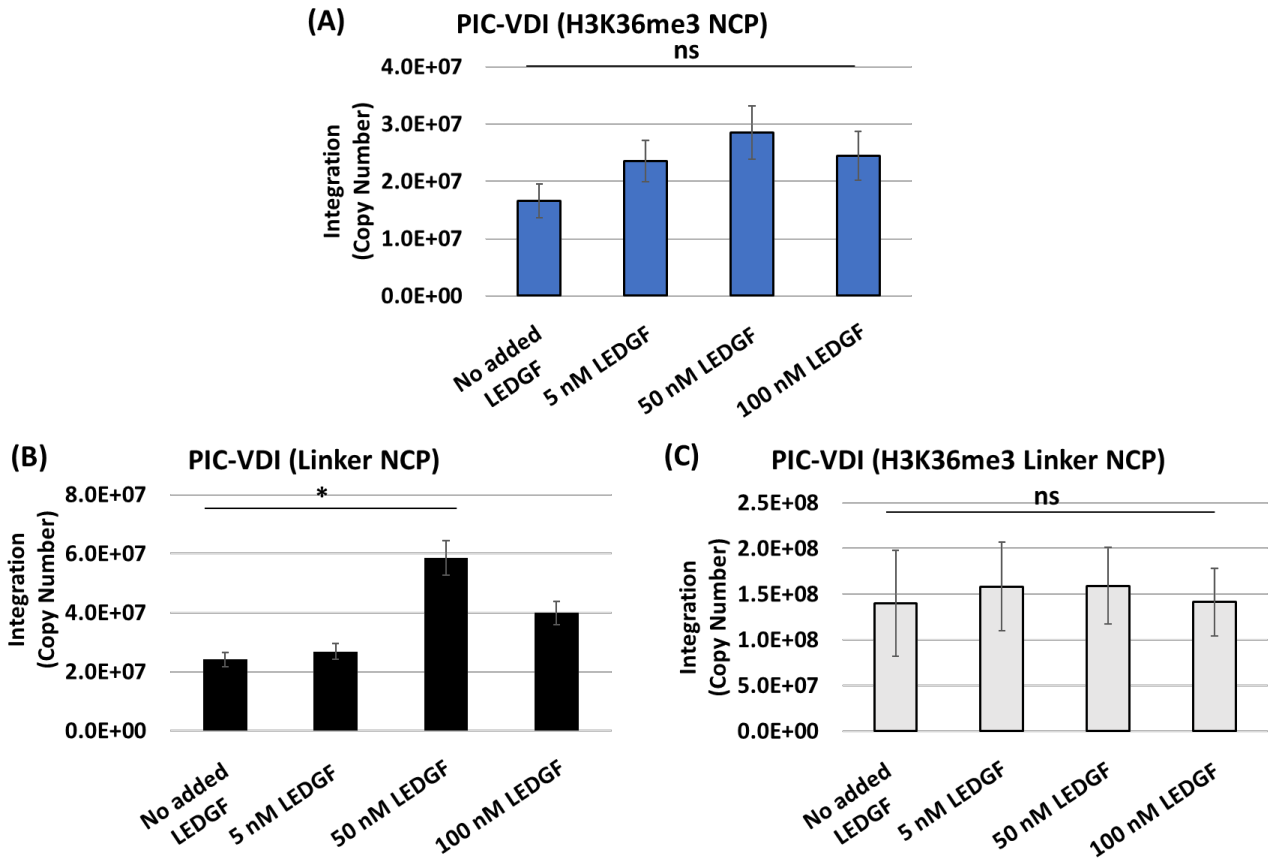

Supplemental Figure 6. The LEDGF/p75 mediated inhibition of PIC-VDI is relieved by the H3K36me3 or the presence of linker DNA. *PIC-mediated integration was measured with H3K36me3 NCPs in the presence of LEDGF/p75 addition. (A) PIC-VDI with H3K36me3-NCP was measured in the presence of LEDGF/p75 addition [5, 50 and 100 nM]. (B-C) PIC-VDI was measured with LEDGF/p75 addition to the linker-NCP and linker-H3K36me3-NCP substrates. These data are shown as the mean copy numbers of at least three independent experiments. The error bars were determined from the SEM and * Represents P > 0.05.*

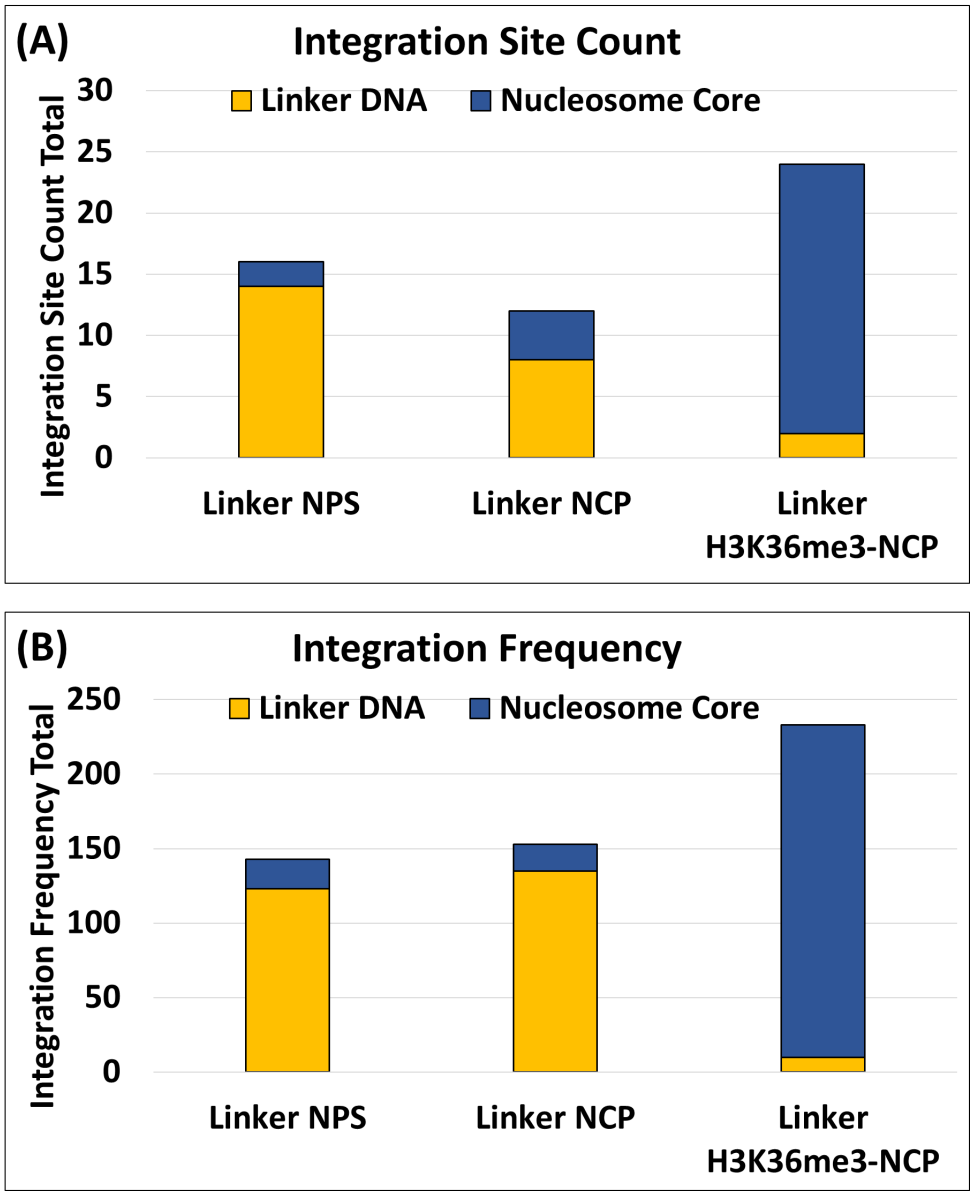

Supplemental Figure 7. PIC-VDI within the linker-H3K36me3-NCP is overrepresented in the nucleosome core compared to the linker-NPS and linker-NCP substrates. *To further study the HIV-1 integration preference within the linker DNA substrates, the DNA from the integration reactions were PCR amplified and subjected to next generation sequencing. Integration sites and frequency at those sites within the linker substrates was determined by quantifying the integration junctions. (A) Quantification of the integration sites within the linker substrates shows the number of integration events (sites) within the linker sequences (1-50 bp and 197-247 bp) and the nucleosome core sequence (50-197 bp). (B) The frequency of integration junctions at a particular site within the sequence was quantified as the integration frequency in the linker sequences and the nucleosome core sequence.*

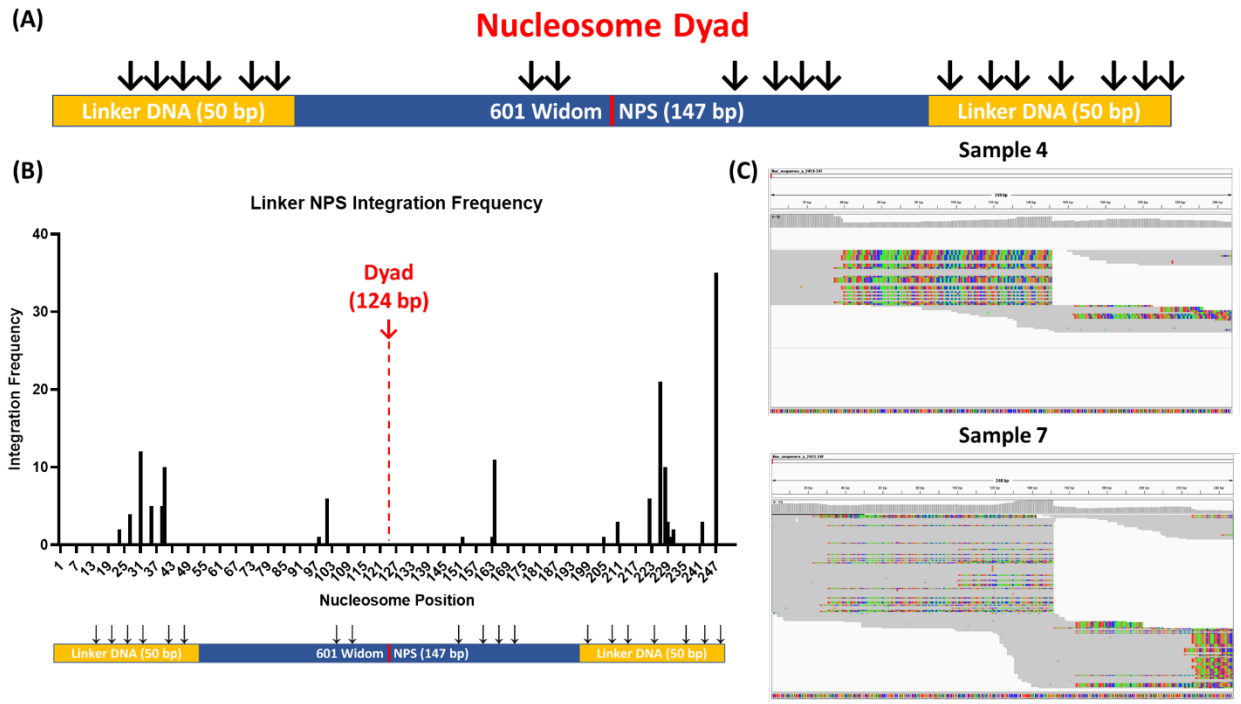

Supplemental Figure 8. Distinct Integration sites with the linker NPS. *The integration frequency within the linker-NPS was determined by quantifying the integration junctions along the substrate sequence. (A) A schematic representation of the integration sites within the linker NPS. (B) The integration frequency is plotted as a histogram for the linker NPS, showing the frequency of integration at particular sites of the substrate. (C) The raw IGV data showing the integration sites within the linker NPS substrate.*

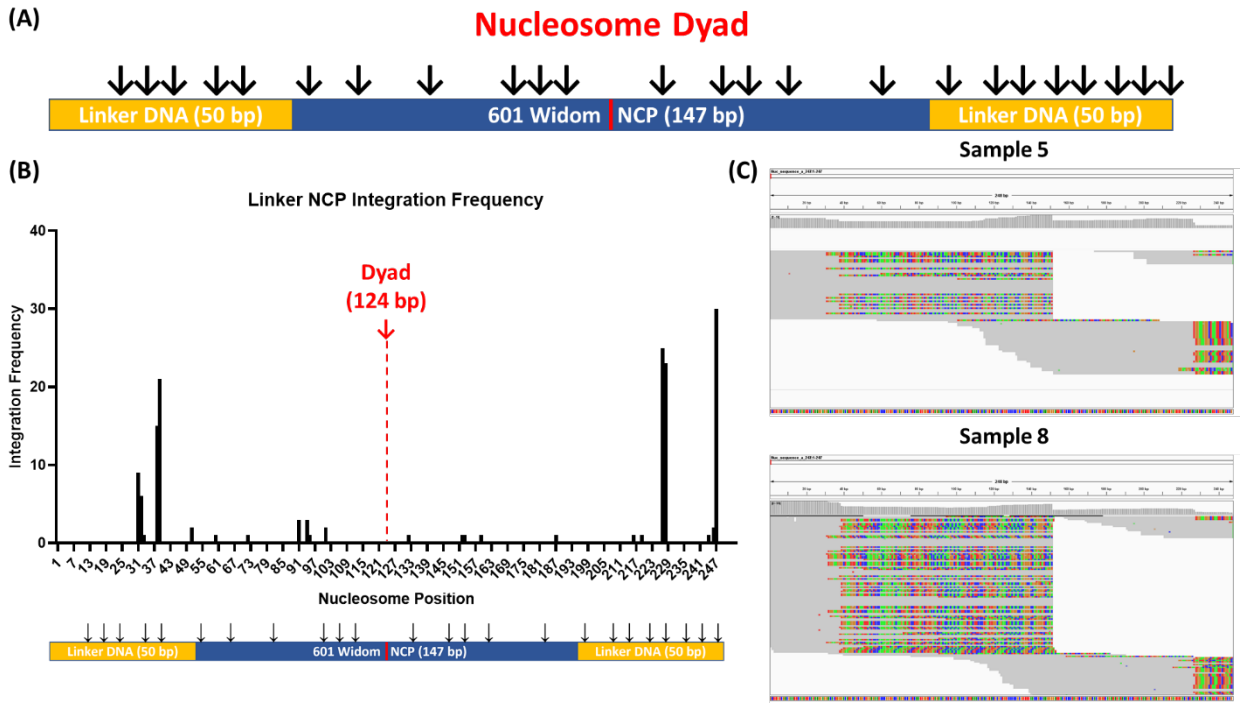

Supplemental Figure 9. Distinct Integration sites with the linker NCP. *The integration frequency with the linker-NCP was determined by quantifying the integration junctions along the substrate sequence. (A) A schematic representation of the integration sites within the linker NCP. (B) The integration frequency is plotted as a histogram for the linker NCP, showing the frequency of integration in specific sites of the substrate. (C) The raw IGV data showing the integration sites within the linker NCP substrate.*

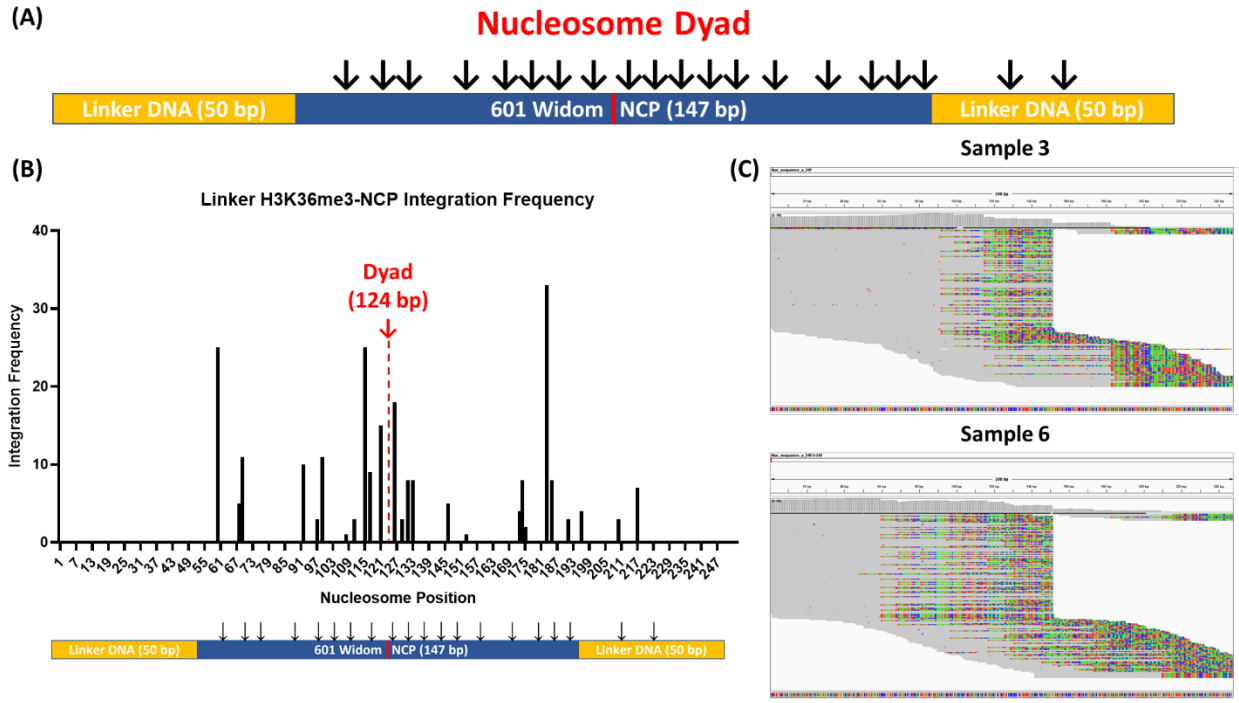

Supplemental Figure 10. Distinct Integration sites with the linker H3K36me3-NCP. *The integration frequency with the linker-H3K36me3-NCP was determined by quantifying the integration junctions along the substrate sequence. (A) A schematic representation of the integration sites within the linker H3K36me3-NCP. (B) The integration frequency is plotted as a histogram for the linker H3K36me3-NCP, showing the frequency of integration in specific sites of the substrate. (C) The raw IGV data showing the integration sites within the linker H3K36me3-NCP substrate.*

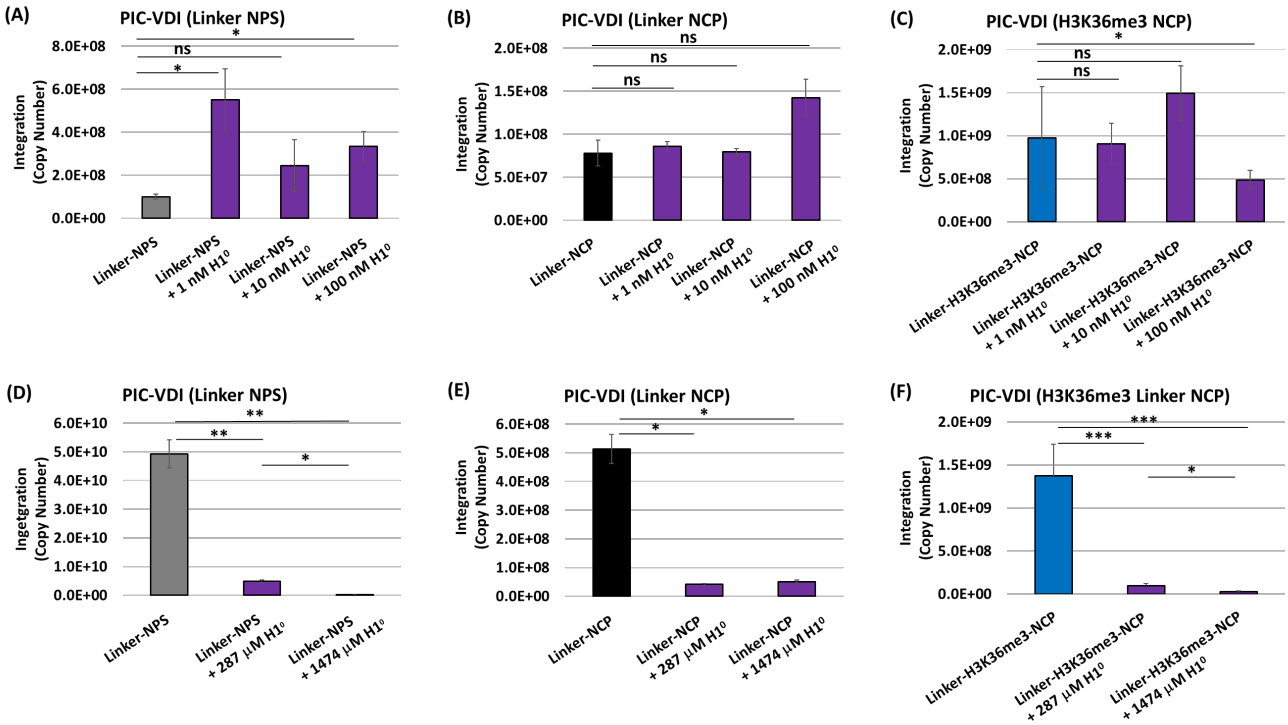

Supplemental Figure 11. Linker histone H1 can inhibit PIC-VDI at saturating concentrations. *The PIC-VDI with the linker substrates was measured with nM amounts of $H1^0$ addition to the assay. (A-C) Non-saturating amounts of $H1^0$ [1, 10 and 100 nM] were added to PIC-VDI with linker-NPS, linker-NCP, and linker-H3K36me3-NCP substrates. The data is represented as the mean of copy number from duplicate experiments. (D-F) The PIC-VDI with saturating amounts of $H1^0$ [247 and 1474 μM] for the linker-NPS, the linker-NCP and the linker-H3K36me3-NCP are represented as the mean of viral DNA copy numbers from at least three independent experiments. For all data, the error bars indicate the standard error mean, and * represents $P > 0.05$, ** $P = 0.01$ to 0.05, *** $P = 0.01$ to 0.001, $P = 0.001$ to 0.0001, **** $P < 0.0001$.*

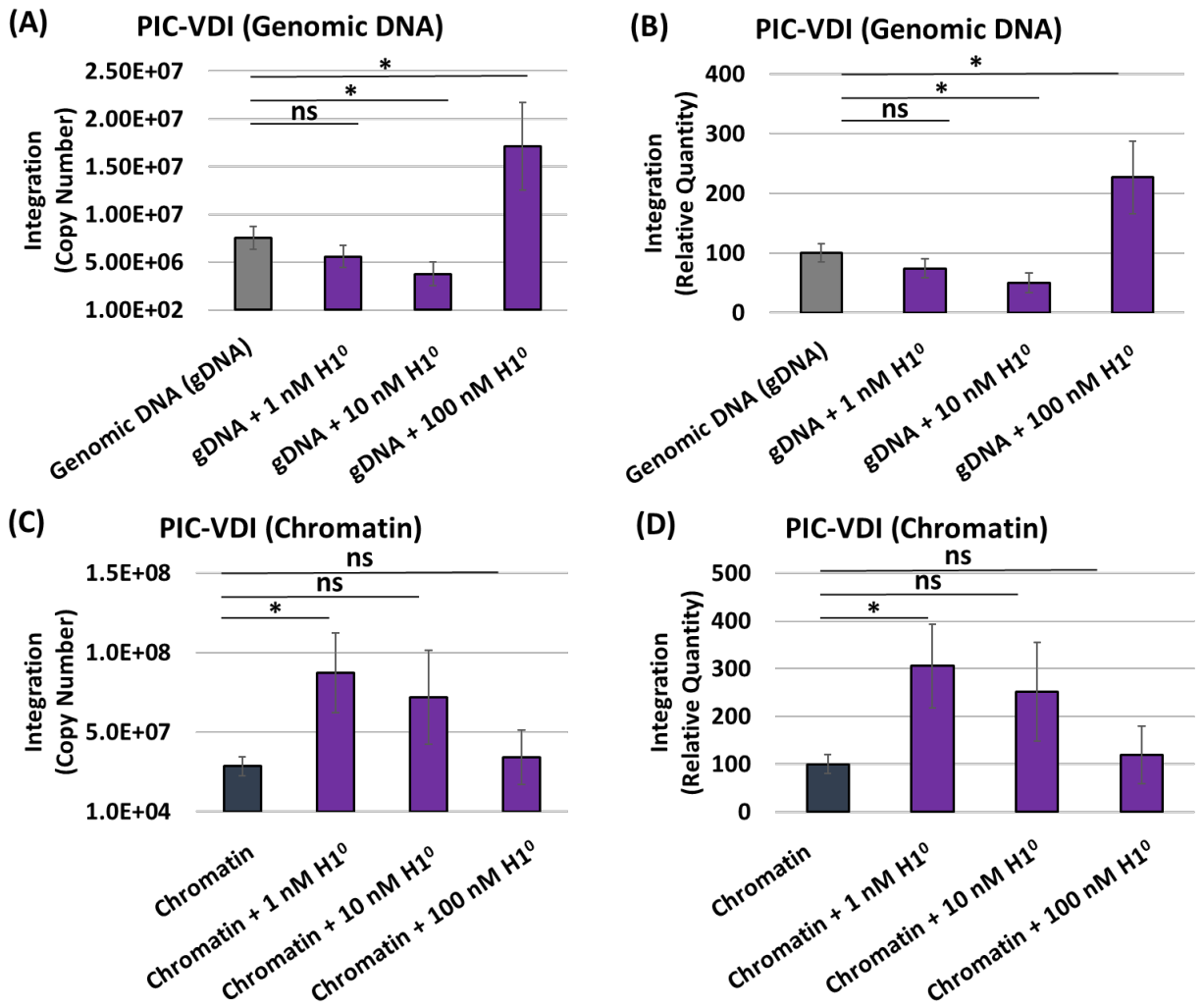

Supplemental Figure 12. Non-saturating H1 addition to genomic DNA and chromatin differentially impacts PIC-VDI. *The PIC-VDI with the genomic DNA (gDNA) and chromatin substrates was measured with nM amounts of $H1^0$ addition to the assay. (A-B) The PIC-VDI with the genomic DNA in the presence of non-saturating amounts of $H1^0$ is represented as the mean copy numbers of independent replicates and as the relative integration quantity. (C-D) The PIC-VDI with non-saturating amounts of $H1^0$ incubated with chromatin is shown as the mean copy number and relative integration quantity. The error bars represent the standard error mean and * represents $P > 0.05$.*

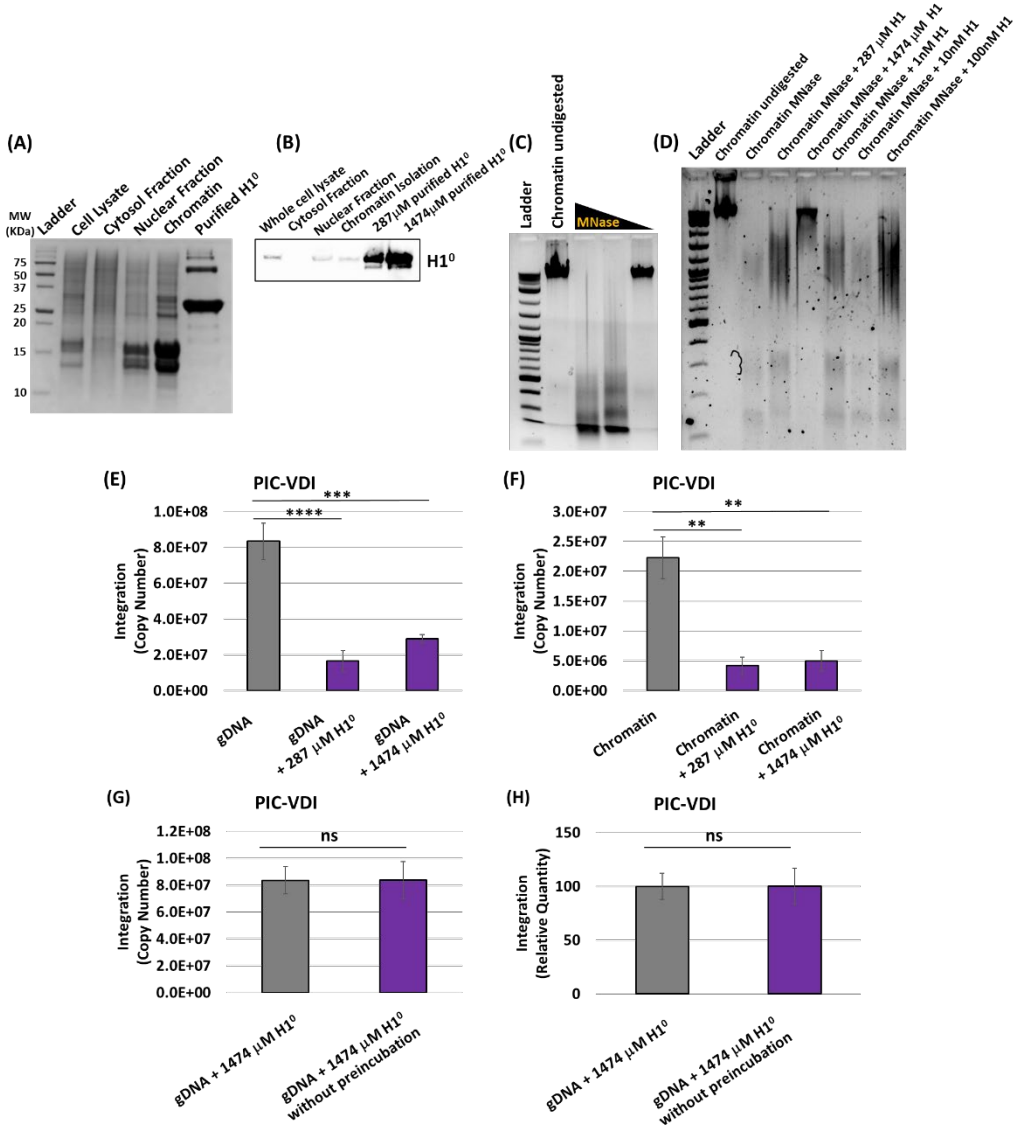

Supplemental Figure 13. Saturation of H1 with chromatin and genomic DNA reduces PIC-VDI. *(A) The purified recombinant $H1^0$ (NEB) was assessed alongside the chromatin isolation fractions by Coomassie staining. (B) Western blot analysis of the chromatin isolation fractions and the saturating amounts of $H1^0$ were probed for H1. (C) Chromatin samples isolated from HEK293T cells were assessed for nucleosome integrity by micrococcal nuclease (MNase) digestion at decreasing amounts. The resultant digested DNA was visualized by ethidium bromide staining of a 1.5 % regular agarose gel. (D) Chromatin samples pre-incubated with various amounts of $H1^0$ were analyzed by MNase digestion and visualized by ethidium bromide staining of a 1.5% agarose gel. (E-F) The PIC-VDI was measured with genomic DNA and chromatin that were incubated on ice with 287 and 1474 μM of $H1^0$ (saturating amounts). The μM concentrations reflect $H1^0$ amounts that are 1:1 and 1:5 (w/w) of DNA substrate to $H1^0$ protein. (G-H) A $H1^0$ time-of-addition experiment with the saturating amount of $H1^0$ is shown comparing the PIC-VDI with gDNA to an assay with $H1^0$ added after the PIC was exposed to the substrate. The PIC-VDI data are represented as the mean of viral DNA copy numbers from at least three independent experiments and the error bars represent the standard error mean. The ** represents P = 0.01 to 0.05, *** P = 0.01 to 0.001, P = 0.001 to 0.0001, **** P < 0.0001.*

Table Supplementary 1.

Sequencing read counts for the PIC integration sites within linker DNA substrates.

Sample Name	Sample #	Reads passing filter	Aligned reads
Linker NPS	4	268	57
	7	440	194
Linker NCP	5	188	80
	8	620	250
Linker H3K36me3 NCP	3	536	359
	6	770	488

Table Supplementary 2.

Primers used in this study.

Primer Name	Sequence (5'-3')	Binding Site	Primer Use
PIC-VDI (REV)	GTGCGCGCTTCAGCAAG	*U5* of HIV-1 genome	PIC-VDI (ALL)
INS-VDI primer	AGCGTGGGCGGGAAAATCTC	INS donor DNA	INS-VDI (ALL)
Gag-PVI (REV)	GTTCCTGCTATGTCACTTCC	HIV-1 *Gag* sequence	
ALU (FWD)	GCCTCCCAAAGTGCTGGGATTACAG	*Alu* repeat in the human genome	PIC-VDI and INS-VDI with chromatin/genomic DNA
NPS-147-FWD	CTGGAGAATCCCGGTGC	5'-end of the Widom 601 NPS	PIC-VDI and INS-VDI with 147 bp Widom substrates
NPS-147-REV	ACAGGATGTATATATCTGACACGTG	3'-end of the Widom 601 NPS	PIC-VDI and INS-VDI with 147 bp Widom substrates
NPS-247-FWD	GCTTGTCGACGAATTCAGATTCATAAGG	5'-end of the linker DNA containing Widom 601 NPS	PIC-VDI and INS-VDI with 247 bp Widom substrates
NPS-247-REV	CGGATCCAGAATTCGTGATTGTAGC	3'-end of the linker DNA containing Widom 601 NPS	PIC-VDI with 247 bp Widom substrates
2nd Round-LTR-F (989)	TCTGGCTAACTAGGGAACCCA	*R* region of HIV-1 genome (LTR)	2ND round qPCR for PIC-VDI and PVI
2nd Round-LTR-R (990)	CTGACTAAAAGGGTCTGAGG	*U5* region of HIV-1 genome (LTR)	2ND round qPCR for PIC-VDI and PVI
2nd Round-LTR-Probe (995)	[6-FAM]-TTAAGCCTCAATAAAGCTTGCCTTGAGTGC-[TAMRA]	*LTR* of HIV-1 genome	2ND round qPCR for PIC-VDI and PVI
2nd Round-Gag-F2	TCAGCCCAGAAGTAATAC	*Gag* of HIV-1 genome	*Gag* specific PVI
2nd Round-Gag-R2	CACTGGATGCAATCTATC	*Gag* of HIV-1 genome	*Gag* specific PVI
2nd Round-Gag-Probe	[FAM]-TCAGCATTATCAGAAGGAGCCACC-[TAMRA]	*Gag* of HIV-1 genome	*Gag* specific PVI
siRNA	CGCGCCAGTCCATTCAGAAGTATAT	*$H1^0$ gene*	Knockdown of *$H1^0$ gene*
siRNA	CAGAAGTATATCAAGAGCCACTACA	*$H1^0$ gene*	Knockdown of *$H1^0$ gene*

References

1 Chawla, A. *et al.* A Review of Long-Term Toxicity of Antiretroviral Treatment Regimens and Implications for an Aging Population. *Infect Dis Ther* **7**, 183-195, doi:10.1007/s40121-018-0201-6 (2018).

2 Craigie, R. & Bushman, F. D. HIV DNA integration. *Cold Spring Harb Perspect Med* **2**, a006890-a006890, doi:10.1101/cshperspect.a006890 (2012).

3 Lesbats, P., Engelman, A. N. & Cherepanov, P. Retroviral DNA Integration. *Chemical Reviews* **116**, 12730-12757, doi:10.1021/acs.chemrev.6b00125 (2016).

4 Maertens, G. N., Engelman, A. N. & Cherepanov, P. Structure and function of retroviral integrase. *Nat Rev Microbiol* **20**, 20-34, doi:10.1038/s41579-021-00586-9 (2022).

5 Craigie, R. Nucleoprotein Intermediates in HIV-1 DNA Integration: Structure and Function of HIV-1 Intasomes. *Subcell Biochem* **88**, 189-210, doi:10.1007/978-981-10-8456-0_9 (2018).

6 Engelman, A., Mizuuchi, K. & Craigie, R. HIV-1 DNA integration: mechanism of viral DNA cleavage and DNA strand transfer. *Cell* **67**, 1211-1221, doi:10.1016/0092-8674(91)90297-c (1991).

7 Bushman, F. D. & Craigie, R. Activities of human immunodeficiency virus (HIV) integration protein in vitro: specific cleavage and integration of HIV DNA. *Proc Natl Acad Sci U S A* **88**, 1339-1343, doi:10.1073/pnas.88.4.1339 (1991).

8 Fujiwara, T. & Mizuuchi, K. Retroviral DNA integration: structure of an integration intermediate. *Cell* **54**, 497-504, doi:10.1016/0092-8674(88)90071-2 (1988).

9 Brown, P. O., Bowerman, B., Varmus, H. E. & Bishop, J. M. Retroviral integration: structure of the initial covalent product and its precursor, and a role for the viral IN protein. *Proc Natl Acad Sci U S A* **86**, 2525-2529, doi:10.1073/pnas.86.8.2525 (1989).

10 Bowerman, B., Brown, P. O., Bishop, J. M. & Varmus, H. E. A nucleoprotein complex mediates the integration of retroviral DNA. *Genes Dev* **3**, 469-478, doi:10.1101/gad.3.4.469 (1989).

11 Farnet, C. M. & Haseltine, W. A. Integration of human immunodeficiency virus type 1 DNA in vitro. *Proc Natl Acad Sci U S A* **87**, 4164-4168, doi:10.1073/pnas.87.11.4164 (1990).

12 Farnet, C. M. & Haseltine, W. A. Determination of viral proteins present in the human immunodeficiency virus type 1 preintegration complex. *J Virol* **65**, 1910-1915, doi:10.1128/JVI.65.4.1910-1915.1991 (1991).

13 Bukrinsky, M. I. *et al.* Association of integrase, matrix, and reverse transcriptase antigens of human immunodeficiency virus type 1 with viral nucleic acids following acute infection. *Proc Natl Acad Sci U S A* **90**, 6125-6129, doi:10.1073/pnas.90.13.6125 (1993).

14 Ellison, V. & Brown, P. O. A stable complex between integrase and viral DNA ends mediates human immunodeficiency virus integration in vitro. *Proc Natl Acad Sci U S A* **91**, 7316-7320, doi:10.1073/pnas.91.15.7316 (1994).

15 Harris, D. & Engelman, A. Both the structure and DNA binding function of the barrier-to-autointegration factor contribute to reconstitution of HIV type 1 integration in vitro. *J Biol Chem* **275**, 39671-39677, doi:10.1074/jbc.M002626200 (2000).

16 Deeks, S. G. *et al.* Research priorities for an HIV cure: International AIDS Society Global Scientific Strategy 2021. *Nature Medicine* **27**, 2085-2098, doi:10.1038/s41591-021-01590-5 (2021).

17 Chun, T. W. *et al.* Presence of an inducible HIV-1 latent reservoir during highly active antiretroviral therapy. *Proc Natl Acad Sci U S A* **94**, 13193-13197, doi:10.1073/pnas.94.24.13193 (1997).

18 Chun, T. W. & Fauci, A. S. HIV reservoirs: pathogenesis and obstacles to viral eradication and cure. *AIDS* **26**, 1261-1268, doi:10.1097/QAD.0b013e328353f3f1 (2012).

19 Schroder, A. R. *et al.* HIV-1 integration in the human genome favors active genes and local hotspots. *Cell* **110**, 521-529, doi:10.1016/s0092-8674(02)00864-4 (2002).
20 Mitchell, R. S. *et al.* Retroviral DNA integration: ASLV, HIV, and MLV show distinct target site preferences. *PLoS Biol* **2**, E234, doi:10.1371/journal.pbio.0020234 (2004).
21 Wang, G. P., Ciuffi, A., Leipzig, J., Berry, C. C. & Bushman, F. D. HIV integration site selection: analysis by massively parallel pyrosequencing reveals association with epigenetic modifications. *Genome Res* **17**, 1186-1194, doi:10.1101/gr.6286907 (2007).
22 Brady, T. *et al.* HIV integration site distributions in resting and activated CD4+ T cells infected in culture. *AIDS* **23**, 1461-1471, doi:10.1097/QAD.0b013e32832caf28 (2009).
23 Wang, G. P. *et al.* Analysis of lentiviral vector integration in HIV+ study subjects receiving autologous infusions of gene modified CD4+ T cells. *Mol Ther* **17**, 844-850, doi:10.1038/mt.2009.16 (2009).
24 Cattoglio, C. *et al.* High-definition mapping of retroviral integration sites identifies active regulatory elements in human multipotent hematopoietic progenitors. *Blood* **116**, 5507-5517, doi:10.1182/blood-2010-05-283523 (2010).
25 Roth, S. L., Malani, N. & Bushman, F. D. Gammaretroviral integration into nucleosomal target DNA in vivo. *J Virol* **85**, 7393-7401, doi:10.1128/jvi.00635-11 (2011).
26 Marini, B. *et al.* Nuclear architecture dictates HIV-1 integration site selection. *Nature* **521**, 227-231, doi:10.1038/nature14226 (2015).
27 Bedwell, G. J., Jang, S., Li, W., Singh, P. K. & Engelman, Alan N. rigrag: high-resolution mapping of genic targeting preferences during HIV-1 integration in vitro and in vivo. *Nucleic Acids Research* **49**, 7330-7346, doi:10.1093/nar/gkab514 (2021).
28 Albanese, A., Arosio, D., Terreni, M. & Cereseto, A. HIV-1 Pre-Integration Complexes Selectively Target Decondensed Chromatin in the Nuclear Periphery. *PLOS ONE* **3**, e2413, doi:10.1371/journal.pone.0002413 (2008).
29 Lelek, M. *et al.* Chromatin organization at the nuclear pore favours HIV replication. *Nature Communications* **6**, 6483, doi:10.1038/ncomms7483 (2015).
30 Sowd, G. A. *et al.* A critical role for alternative polyadenylation factor CPSF6 in targeting HIV-1 integration to transcriptionally active chromatin. *Proc Natl Acad Sci U S A* **113**, E1054-1063, doi:10.1073/pnas.1524213113 (2016).
31 Lucic, B. *et al.* Spatially clustered loci with multiple enhancers are frequent targets of HIV-1 integration. *Nature Communications* **10**, 4059, doi:10.1038/s41467-019-12046-3 (2019).
32 Battivelli, E. *et al.* Distinct chromatin functional states correlate with HIV latency reactivation in infected primary CD4(+) T cells. *Elife* **7**, doi:10.7554/eLife.34655 (2018).
33 Cohn, L. B. *et al.* HIV-1 integration landscape during latent and active infection. *Cell* **160**, 420-432, doi:10.1016/j.cell.2015.01.020 (2015).
34 McGinty, R. K. & Tan, S. Nucleosome Structure and Function. *Chemical Reviews* **115**, 2255-2273, doi:10.1021/cr500373h (2015).
35 Luger, K., Mader, A. W., Richmond, R. K., Sargent, D. F. & Richmond, T. J. Crystal structure of the nucleosome core particle at 2.8 A resolution. *Nature* **389**, 251-260, doi:10.1038/38444 (1997).
36 Simpson, R. T. Structure of the chromatosome, a chromatin particle containing 160 base pairs of DNA and all the histones. *Biochemistry* **17**, 5524-5531, doi:10.1021/bi00618a030 (1978).
37 Allan, J., Hartman, P. G., Crane-Robinson, C. & Aviles, F. X. The structure of histone H1 and its location in chromatin. *Nature* **288**, 675-679, doi:10.1038/288675a0 (1980).
38 Woodcock, C. L., Skoultchi, A. I. & Fan, Y. Role of linker histone in chromatin structure and function: H1 stoichiometry and nucleosome repeat length. *Chromosome Res* **14**, 17-25, doi:10.1007/s10577-005-1024-3 (2006).
39 Bowman, G. D. & Poirier, M. G. Post-translational modifications of histones that influence nucleosome dynamics. *Chem Rev* **115**, 2274-2295, doi:10.1021/cr500350x (2015).

40 Allis, C. D. & Jenuwein, T. The molecular hallmarks of epigenetic control. *Nat Rev Genet* **17**, 487-500, doi:10.1038/nrg.2016.59 (2016).
41 Fierz, B. & Poirier, M. G. Biophysics of Chromatin Dynamics. *Annu Rev Biophys* **48**, 321-345, doi:10.1146/annurev-biophys-070317-032847 (2019).
42 Pryciak, P. M., Muller, H. P. & Varmus, H. E. Simian virus 40 minichromosomes as targets for retroviral integration in vivo. *Proc Natl Acad Sci U S A* **89**, 9237-9241, doi:10.1073/pnas.89.19.9237 (1992).
43 Pryciak, P. M., Sil, A. & Varmus, H. E. Retroviral integration into minichromosomes in vitro. *EMBO J* **11**, 291-303 (1992).
44 Pryciak, P. M. & Varmus, H. E. Nucleosomes, DNA-binding proteins, and DNA sequence modulate retroviral integration target site selection. *Cell* **69**, 769-780, doi:10.1016/0092-8674(92)90289-o (1992).
45 Pruss, D., Bushman, F. D. & Wolffe, A. P. Human immunodeficiency virus integrase directs integration to sites of severe DNA distortion within the nucleosome core. *Proc Natl Acad Sci U S A* **91**, 5913-5917, doi:10.1073/pnas.91.13.5913 (1994).
46 Pruss, D., Reeves, R., Bushman, F. D. & Wolffe, A. P. The influence of DNA and nucleosome structure on integration events directed by HIV integrase. *J Biol Chem* **269**, 25031-25041 (1994).
47 Muller, H. P. & Varmus, H. E. DNA bending creates favored sites for retroviral integration: an explanation for preferred insertion sites in nucleosomes. *EMBO J* **13**, 4704-4714 (1994).
48 Taganov, K. D. *et al.* Integrase-specific enhancement and suppression of retroviral DNA integration by compacted chromatin structure in vitro. *J Virol* **78**, 5848-5855, doi:10.1128/JVI.78.11.5848-5855.2004 (2004).
49 Botbol, Y., Raghavendra, N. K., Rahman, S., Engelman, A. & Lavigne, M. Chromatinized templates reveal the requirement for the LEDGF/p75 PWWP domain during HIV-1 integration in vitro. *Nucleic acids research* **36**, 1237-1246, doi:10.1093/nar/gkm1127 (2008).
50 Benleulmi, M. S. *et al.* Intasome architecture and chromatin density modulate retroviral integration into nucleosome. *Retrovirology* **12**, 13, doi:10.1186/s12977-015-0145-9 (2015).
51 Lapaillerie, D. *et al.* Modulation of the intrinsic chromatin binding property of HIV-1 integrase by LEDGF/p75. *Nucleic Acids Research* **49**, 11241-11256, doi:10.1093/nar/gkab886 (2021).
52 Cosnefroy, O. *et al.* Stimulation of the human RAD51 nucleofilament restricts HIV-1 integration in vitro and in infected cells. *J Virol* **86**, 513-526, doi:10.1128/jvi.05425-11 (2012).
53 Matysiak, J. *et al.* Modulation of chromatin structure by the FACT histone chaperone complex regulates HIV-1 integration. *Retrovirology* **14**, 39, doi:10.1186/s12977-017-0363-4 (2017).
54 Mauro, E. *et al.* Human H4 tail stimulates HIV-1 integration through binding to the carboxy-terminal domain of integrase. *Nucleic Acids Res* **47**, 3607-3618, doi:10.1093/nar/gkz091 (2019).
55 Lesbats, P. *et al.* Functional coupling between HIV-1 integrase and the SWI/SNF chromatin remodeling complex for efficient in vitro integration into stable nucleosomes. *PLoS Pathog* **7**, e1001280, doi:10.1371/journal.ppat.1001280 (2011).
56 Gupta, S. S. *et al.* Bromo- and extraterminal domain chromatin regulators serve as cofactors for murine leukemia virus integration. *J Virol* **87**, 12721-12736, doi:10.1128/jvi.01942-13 (2013).
57 Debyser, Z., Christ, F., De Rijck, J. & Gijsbers, R. Host factors for retroviral integration site selection. *Trends Biochem Sci* **40**, 108-116, doi:10.1016/j.tibs.2014.12.001 (2015).

58 Naughtin, M. *et al.* DNA Physical Properties and Nucleosome Positions Are Major Determinants of HIV-1 Integrase Selectivity. *PLOS ONE* **10**, e0129427, doi:10.1371/journal.pone.0129427 (2015).
59 Cherepanov, P. *et al.* HIV-1 integrase forms stable tetramers and associates with LEDGF/p75 protein in human cells. *J Biol Chem* **278**, 372-381, doi:10.1074/jbc.M209278200 (2003).
60 Ciuffi, A. *et al.* A role for LEDGF/p75 in targeting HIV DNA integration. *Nat Med* **11**, 1287-1289, doi:10.1038/nm1329 (2005).
61 Emiliani, S. *et al.* Integrase mutants defective for interaction with LEDGF/p75 are impaired in chromosome tethering and HIV-1 replication. *J Biol Chem* **280**, 25517-25523, doi:10.1074/jbc.M501378200 (2005).
62 Llano, M. *et al.* An essential role for LEDGF/p75 in HIV integration. *Science* **314**, 461-464, doi:10.1126/science.1132319 (2006).
63 Llano, M. *et al.* Identification and characterization of the chromatin-binding domains of the HIV-1 integrase interactor LEDGF/p75. *J Mol Biol* **360**, 760-773, doi:10.1016/j.jmb.2006.04.073 (2006).
64 Vandegraaff, N., Devroe, E., Turlure, F., Silver, P. A. & Engelman, A. Biochemical and genetic analyses of integrase-interacting proteins lens epithelium-derived growth factor (LEDGF)/p75 and hepatoma-derived growth factor related protein 2 (HRP2) in preintegration complex function and HIV-1 replication. *Virology* **346**, 415-426, doi:10.1016/j.virol.2005.11.022 (2006).
65 Vandekerckhove, L. *et al.* Transient and stable knockdown of the integrase cofactor LEDGF/p75 reveals its role in the replication cycle of human immunodeficiency virus. *J Virol* **80**, 1886-1896, doi:10.1128/jvi.80.4.1886-1896.2006 (2006).
66 Cherepanov, P. LEDGF/p75 interacts with divergent lentiviral integrases and modulates their enzymatic activity in vitro. *Nucleic Acids Res* **35**, 113-124, doi:10.1093/nar/gkl885 (2007).
67 Hombrouck, A. *et al.* Virus evolution reveals an exclusive role for LEDGF/p75 in chromosomal tethering of HIV. *PLoS Pathog* **3**, e47, doi:10.1371/journal.ppat.0030047 (2007).
68 Marshall, H. M. *et al.* Role of PSIP1/LEDGF/p75 in lentiviral infectivity and integration targeting. *PLoS One* **2**, e1340, doi:10.1371/journal.pone.0001340 (2007).
69 Shun, M. C. *et al.* LEDGF/p75 functions downstream from preintegration complex formation to effect gene-specific HIV-1 integration. *Genes Dev* **21**, 1767-1778, doi:10.1101/gad.1565107 (2007).
70 Engelman, A. & Cherepanov, P. The lentiviral integrase binding protein LEDGF/p75 and HIV-1 replication. *PLoS Pathog* **4**, e1000046, doi:10.1371/journal.ppat.1000046 (2008).
71 Addai, A. B. *et al.* Cocaine modulates HIV-1 integration in primary CD4+ T cells: implications in HIV-1 pathogenesis in drug-abusing patients. *J Leukoc Biol* **97**, 779-790, doi:10.1189/jlb.4A0714-356R (2015).
72 Balasubramaniam, M., Davids, B., Addai, A. B., Pandhare, J. & Dash, C. Measurement of In Vitro Integration Activity of HIV-1 Preintegration Complexes. *J Vis Exp*, doi:10.3791/54581 (2017).
73 Balasubramaniam, M. *et al.* PF74 Inhibits HIV-1 Integration by Altering the Composition of the Preintegration Complex. *J Virol* **93**, doi:10.1128/jvi.01741-18 (2019).
74 Davids, B. O. *et al.* Human Three Prime Repair Exonuclease 1 Promotes HIV-1 Integration by Preferentially Degrading Unprocessed Viral DNA. *J Virol* **95**, e0055521, doi:10.1128/jvi.00555-21 (2021).
75 van Holde, K. E. *Chromatin*. Vol. 1 (Springer, New York, NY, 1989).
76 Maskell, D. P. *et al.* Structural basis for retroviral integration into nucleosomes. *Nature* **523**, 366-369, doi:10.1038/nature14495 (2015).

77 Luger, K., Rechsteiner, T. J. & Richmond, T. J. in *Methods in Enzymology* Vol. 304 3-19 (Academic Press, 1999).
78 Lowary, P. T. & Widom, J. New DNA sequence rules for high affinity binding to histone octamer and sequence-directed nucleosome positioning. *J Mol Biol* **276**, 19-42, doi:10.1006/jmbi.1997.1494 (1998).
79 Christensen, D. E., Ganser-Pornillos, B. K., Johnson, J. S., Pornillos, O. & Sundquist, W. I. Reconstitution and visualization of HIV-1 capsid-dependent replication and integration in vitro. *Science* **370**, eabc8420, doi:doi:10.1126/science.abc8420 (2020).
80 Thåström, A. *et al.* Sequence motifs and free energies of selected natural and non-natural nucleosome positioning DNA sequences. *J Mol Biol* **288**, 213-229, doi:10.1006/jmbi.1999.2686 (1999).
81 Li, M. & Craigie, R. Nucleoprotein complex intermediates in HIV-1 integration. *Methods* **47**, 237-242, doi:10.1016/j.ymeth.2009.02.001 (2009).
82 Li, M., Jurado, K. A., Lin, S., Engelman, A. & Craigie, R. Engineered hyperactive integrase for concerted HIV-1 DNA integration. *PLoS One* **9**, e105078, doi:10.1371/journal.pone.0105078 (2014).
83 Young, N. L. *et al.* High throughput characterization of combinatorial histone codes. *Mol Cell Proteomics* **8**, 2266-2284, doi:10.1074/mcp.M900238-MCP200 (2009).
84 Rando, O. J. Combinatorial complexity in chromatin structure and function: revisiting the histone code. *Curr Opin Genet Dev* **22**, 148-155, doi:10.1016/j.gde.2012.02.013 (2012).
85 Wu, V. H. *et al.* Assessment of HIV-1 integration in tissues and subsets across infection stages. *JCI Insight* **5**, doi:10.1172/jci.insight.139783 (2020).
86 Musselman, C. A. *et al.* Binding of PHF1 Tudor to H3K36me3 enhances nucleosome accessibility. *Nat Commun* **4**, 2969, doi:10.1038/ncomms3969 (2013).
87 Simon, M. D. *et al.* The Site-Specific Installation of Methyl-Lysine Analogs into Recombinant Histones. *Cell* **128**, 1003-1012, doi:10.1016/j.cell.2006.12.041 (2007).
88 Kvaratskhelia, M., Sharma, A., Larue, R. C., Serrao, E. & Engelman, A. Molecular mechanisms of retroviral integration site selection. *Nucleic Acids Research* **42**, 10209-10225, doi:10.1093/nar/gku769 (2014).
89 Lusic, M. & Siliciano, R. F. Nuclear landscape of HIV-1 infection and integration. *Nat Rev Microbiol* **15**, 69-82, doi:10.1038/nrmicro.2016.162 (2017).
90 Engelman, A. N. & Singh, P. K. Cellular and molecular mechanisms of HIV-1 integration targeting. *Cell Mol Life Sci* **75**, 2491-2507, doi:10.1007/s00018-018-2772-5 (2018).
91 Poletti, V. & Mavilio, F. Interactions between Retroviruses and the Host Cell Genome. *Molecular Therapy - Methods & Clinical Development* **8**, 31-41, doi:10.1016/j.omtm.2017.10.001 (2018).
92 Cherepanov, P., Devroe, E., Silver, P. A. & Engelman, A. Identification of an evolutionarily conserved domain in human lens epithelium-derived growth factor/transcriptional co-activator p75 (LEDGF/p75) that binds HIV-1 integrase. *J Biol Chem* **279**, 48883-48892, doi:10.1074/jbc.M406307200 (2004).
93 Cherepanov, P. *et al.* Solution structure of the HIV-1 integrase-binding domain in LEDGF/p75. *Nat Struct Mol Biol* **12**, 526-532, doi:10.1038/nsmb937 (2005).
94 Vanegas, M. *et al.* Identification of the LEDGF/p75 HIV-1 integrase-interaction domain and NLS reveals NLS-independent chromatin tethering. *J Cell Sci* **118**, 1733-1743, doi:10.1242/jcs.02299 (2005).
95 Shimko, J. C., North, J. A., Bruns, A. N., Poirier, M. G. & Ottesen, J. J. Preparation of fully synthetic histone H3 reveals that acetyl-lysine 56 facilitates protein binding within nucleosomes. *J Mol Biol* **408**, 187-204, doi:10.1016/j.jmb.2011.01.003 (2011).
96 Le, J. V. *et al.* Probing Nucleosome Stability with a DNA Origami Nanocaliper. *ACS Nano* **10**, 7073-7084, doi:10.1021/acsnano.6b03218 (2016).

97 Eidahl, J. O. *et al.* Structural basis for high-affinity binding of LEDGF PWWP to mononucleosomes. *Nucleic Acids Res* **41**, 3924-3936, doi:10.1093/nar/gkt074 (2013).
98 Wang, H., Farnung, L., Dienemann, C. & Cramer, P. Structure of H3K36-methylated nucleosome-PWWP complex reveals multivalent cross-gyre binding. *Nat Struct Mol Biol* **27**, 8-13, doi:10.1038/s41594-019-0345-4 (2020).
99 Compton, J. L., Bellard, M. & Chambon, P. Biochemical evidence of variability in the DNA repeat length in the chromatin of higher eukaryotes. *Proc Natl Acad Sci U S A* **73**, 4382-4386, doi:10.1073/pnas.73.12.4382 (1976).
100 Robinson, P. J. & Rhodes, D. Structure of the '30 nm' chromatin fibre: a key role for the linker histone. *Curr Opin Struct Biol* **16**, 336-343, doi:10.1016/j.sbi.2006.05.007 (2006).
101 Bednar, J. *et al.* Structure and Dynamics of a 197 bp Nucleosome in Complex with Linker Histone H1. *Mol Cell* **66**, 384-397 e388, doi:10.1016/j.molcel.2017.04.012 (2017).
102 Chaudhuri, E. *et al.* The HIV-1 capsid-binding host factor CPSF6 is post-transcriptionally regulated by the cellular microRNA miR-125b. *J Biol Chem* **295**, 5081-5094, doi:10.1074/jbc.RA119.010534 (2020).
103 Benleulmi, M. S. *et al.* Modulation of the functional association between the HIV-1 intasome and the nucleosome by histone amino-terminal tails. *Retrovirology* **14**, 54, doi:10.1186/s12977-017-0378-x (2017).
104 Chereji, R. V., Bryson, T. D. & Henikoff, S. Quantitative MNase-seq accurately maps nucleosome occupancy levels. *Genome Biology* **20**, 198, doi:10.1186/s13059-019-1815-z (2019).
105 Knezetic, J. A. & Luse, D. S. The presence of nucleosomes on a DNA template prevents initiation by RNA polymerase II in vitro. *Cell* **45**, 95-104, doi:10.1016/0092-8674(86)90541-6 (1986).
106 Lorch, Y., LaPointe, J. W. & Kornberg, R. D. Nucleosomes inhibit the initiation of transcription but allow chain elongation with the displacement of histones. *Cell* **49**, 203-210, doi:10.1016/0092-8674(87)90561-7 (1987).
107 Ehrenhofer-Murray, A. E. Chromatin dynamics at DNA replication, transcription and repair. *European Journal of Biochemistry* **271**, 2335-2349, doi:https://doi.org/10.1111/j.1432-1033.2004.04162.x (2004).
108 Ransom, M., Dennehey, B. K. & Tyler, J. K. Chaperoning histones during DNA replication and repair. *Cell* **140**, 183-195, doi:10.1016/j.cell.2010.01.004 (2010).
109 Lai, W. K. M. & Pugh, B. F. Understanding nucleosome dynamics and their links to gene expression and DNA replication. *Nature reviews. Molecular cell biology* **18**, 548-562, doi:10.1038/nrm.2017.47 (2017).
110 Pasi, M. *et al.* DNA minicircles clarify the specific role of DNA structure on retroviral integration. *Nucleic Acids Res* **44**, 7830-7847, doi:10.1093/nar/gkw651 (2016).
111 Valouev, A. *et al.* Determinants of nucleosome organization in primary human cells. *Nature* **474**, 516-520, doi:10.1038/nature10002 (2011).
112 Frenster, J. H., Allfrey, V. G. & Mirsky, A. E. Repressed and Active Chromatin Isolated from Interphase Lymphocytes. *Proc Natl Acad Sci U S A* **50**, 1026-1032, doi:10.1073/pnas.50.6.1026 (1963).
113 Huisinga, K. L., Brower-Toland, B. & Elgin, S. C. The contradictory definitions of heterochromatin: transcription and silencing. *Chromosoma* **115**, 110-122, doi:10.1007/s00412-006-0052-x (2006).
114 Bannister, A. J. & Kouzarides, T. Regulation of chromatin by histone modifications. *Cell Research* **21**, 381-395, doi:10.1038/cr.2011.22 (2011).
115 Matzke, M. A. & Mosher, R. A. RNA-directed DNA methylation: an epigenetic pathway of increasing complexity. *Nature Reviews Genetics* **15**, 394-408, doi:10.1038/nrg3683 (2014).

116 De Ravin, S. S. *et al.* Enhancers are major targets for murine leukemia virus vector integration. *Journal of virology* **88**, 4504-4513, doi:10.1128/JVI.00011-14 (2014).
117 Ernst, J. *et al.* Mapping and analysis of chromatin state dynamics in nine human cell types. *Nature* **473**, 43-49, doi:10.1038/nature09906 (2011).
118 Chen, E. S. *et al.* Cell cycle control of centromeric repeat transcription and heterochromatin assembly. *Nature* **451**, 734-737, doi:10.1038/nature06561 (2008).
119 Woo, H., Dam Ha, S., Lee, S. B., Buratowski, S. & Kim, T. Modulation of gene expression dynamics by co-transcriptional histone methylations. *Exp Mol Med* **49**, e326, doi:10.1038/emm.2017.19 (2017).
120 Wagner, E. J. & Carpenter, P. B. Understanding the language of Lys36 methylation at histone H3. *Nat Rev Mol Cell Biol* **13**, 115-126, doi:10.1038/nrm3274 (2012).
121 Neri, F. *et al.* Intragenic DNA methylation prevents spurious transcription initiation. *Nature* **543**, 72-77, doi:10.1038/nature21373 (2017).
122 Li, F. *et al.* The histone mark H3K36me3 regulates human DNA mismatch repair through its interaction with MutSα. *Cell* **153**, 590-600, doi:10.1016/j.cell.2013.03.025 (2013).
123 Sundarraj, J., Taylor, G. C. A., von Kriegsheim, A. & Pradeepa, M. M. H3K36me3 and PSIP1/LEDGF associate with several DNA repair proteins, suggesting their role in efficient DNA repair at actively transcribing loci. *Wellcome Open Research* **2**, 83, doi:10.12688/wellcomeopenres.11589.4 (2021).
124 Vansant, G. *et al.* The chromatin landscape at the HIV-1 provirus integration site determines viral expression. *Nucleic Acids Res* **48**, 7801-7817, doi:10.1093/nar/gkaa536 (2020).
125 in *Retroviruses* (eds J. M. Coffin, S. H. Hughes, & H. E. Varmus) (Cold Spring Harbor Laboratory Press

Copyright © 1997, Cold Spring Harbor Laboratory Press., 1997).
126 Bedwell, G. J. & Engelman, A. N. Factors that mold the nuclear landscape of HIV-1 integration. *Nucleic Acids Res* **49**, 621-635, doi:10.1093/nar/gkaa1207 (2021).
127 van Nuland, R. *et al.* Nucleosomal DNA binding drives the recognition of H3K36-methylated nucleosomes by the PSIP1-PWWP domain. *Epigenetics Chromatin* **6**, 12, doi:10.1186/1756-8935-6-12 (2013).
128 Shun, M. C. *et al.* Identification and characterization of PWWP domain residues critical for LEDGF/p75 chromatin binding and human immunodeficiency virus type 1 infectivity. *J Virol* **82**, 11555-11567, doi:10.1128/JVI.01561-08 (2008).
129 Satchwell, S. C., Drew, H. R. & Travers, A. A. Sequence periodicities in chicken nucleosome core DNA. *J Mol Biol* **191**, 659-675, doi:10.1016/0022-2836(86)90452-3 (1986).
130 Chua, E. Y., Vasudevan, D., Davey, G. E., Wu, B. & Davey, C. A. The mechanics behind DNA sequence-dependent properties of the nucleosome. *Nucleic Acids Res* **40**, 6338-6352, doi:10.1093/nar/gks261 (2012).
131 Katzman, M. & Sudol, M. Mapping domains of retroviral integrase responsible for viral DNA specificity and target site selection by analysis of chimeras between human immunodeficiency virus type 1 and visna virus integrases. *J Virol* **69**, 5687-5696, doi:10.1128/jvi.69.9.5687-5696.1995 (1995).
132 Shibagaki, Y. & Chow, S. A. Central core domain of retroviral integrase is responsible for target site selection. *J Biol Chem* **272**, 8361-8369, doi:10.1074/jbc.272.13.8361 (1997).
133 Janssen, A., Colmenares, S. U. & Karpen, G. H. Heterochromatin: Guardian of the Genome. *Annu Rev Cell Dev Biol* **34**, 265-288, doi:10.1146/annurev-cellbio-100617-062653 (2018).

134 Terme, J.-M. *et al.* Histone H1 Variants Are Differentially Expressed and Incorporated into Chromatin during Differentiation and Reprogramming to Pluripotency *. *Journal of Biological Chemistry* **286**, 35347-35357, doi:10.1074/jbc.M111.281923 (2011).
135 Cirillo, L. A. *et al.* Opening of compacted chromatin by early developmental transcription factors HNF3 (FoxA) and GATA-4. *Mol Cell* **9**, 279-289, doi:10.1016/s1097-2765(02)00459-8 (2002).
136 Sancho, M., Diani, E., Beato, M. & Jordan, A. Depletion of Human Histone H1 Variants Uncovers Specific Roles in Gene Expression and Cell Growth. *PLOS Genetics* **4**, e1000227, doi:10.1371/journal.pgen.1000227 (2008).
137 Fan, Y., Sirotkin, A., Russell, R. G., Ayala, J. & Skoultchi, A. I. Individual Somatic H1 Subtypes Are Dispensable for Mouse Development Even in Mice Lacking the H1⁰Replacement Subtype. *Molecular and Cellular Biology* **21**, 7933-7943, doi:doi:10.1128/MCB.21.23.7933-7943.2001 (2001).
138 Bhan, S., May, W., Warren, S. L. & Sittman, D. B. Global gene expression analysis reveals specific and redundant roles for H1 variants, H1c and H10, in gene expression regulation. *Gene* **414**, 10-18, doi:https://doi.org/10.1016/j.gene.2008.01.025 (2008).
139 Platt, E. J., Wehrly, K., Kuhmann, S. E., Chesebro, B. & Kabat, D. Effects of CCR5 and CD4 cell surface concentrations on infections by macrophagetropic isolates of human immunodeficiency virus type 1. *J Virol* **72**, 2855-2864, doi:10.1128/JVI.72.4.2855-2864.1998 (1998).
140 Schnitzler, G. R. Isolation of histones and nucleosome cores from mammalian cells. *Curr Protoc Mol Biol* **Chapter 21**, Unit 21 25, doi:10.1002/0471142727.mb2105s50 (2001).
141 Gibson, M. D., Gatchalian, J., Slater, A., Kutateladze, T. G. & Poirier, M. G. PHF1 Tudor and N-terminal domains synergistically target partially unwrapped nucleosomes to increase DNA accessibility. *Nucleic Acids Res* **45**, 3767-3776, doi:10.1093/nar/gkw1320 (2017).
142 Clegg, R. M. in *Methods in Enzymology* Vol. 211 353-388 (Academic Press, 1992).
143 Robinson, J. T. *et al.* Integrative genomics viewer. *Nat Biotechnol* **29**, 24-26, doi:10.1038/nbt.1754 (2011).